Soot-containing particles in the atmosphere: modifications of morphology and mixing states with water-soluble materials

(大気中のスス含有粒子：形態および水溶性物質との混合状態の変化)

UEDA, Sayako

(上田紗也子)

A dissertation for degree of Doctor of Science

Department of Earth and Environmental Sciences,

Graduate School of Environmental Studies, Nagoya University

（名古屋大学大学院環境学研究科地球環境科学専攻学位論文　博士（理学））

2011

要旨

大気エアロゾル粒子に含まれるススは、大気中の主要な光吸収性物質であり、主に化石燃料の燃焼やバイオマスバーニングによって大気中に放出される。化石燃料の燃焼で排出された直後のスス粒子は疎水性を示すが、硫酸塩などの水溶性物質が付着すると、吸湿性粒子としてふるまう。スス粒子の変質に関わる大気中での主な過程には、低揮発性気体物質の吸着や凝縮、他の粒子との凝集、液滴粒子への溶け込みがある。ススによる気候影響を評価するために、ススを含有する粒子（スス含有粒子）の空間的な濃度分布と光吸収量・散乱量を見積もる必要がある。スス含有粒子の光吸収・散乱特性は、付着物の量や付着物を含めた粒子の形態により異なる。スス粒子の光学特性は変質により変わるため、スス含有粒子の形態的特徴が大気輸送中にどのように変化するかを知ることは重要である。しかし、大気中のスス含有粒子の付着物量と形態とを同時に調べた研究例は少なく、スス含有粒子の変質と粒子形態との関係についての理解は不十分である。一方、スス含有粒子の地理的分布や長距離輸送は、大気中での除去過程に左右される。サブミクロンサイズのスス含有粒子が大気から除去されるには、雲へ取り込まれた後に降水として除去される過程が主要である。サブミクロン粒子の雲凝結核としての機能は、吸湿性の有無で異なる。スス粒子の雲凝結核としての機能は、大気中での変質により高められる。しかし、変質前の疎水性のスス粒子は雲凝結核としての機能に乏しく、雲・降水過程で除去される可能性が低いと予想される。雲・降水過程後に大気に残るスス含有粒子の性質や量を考える上で、実際の雲内で雲粒に取り込まれないスス含有粒子の吸湿性の有無に関する情報が必要である。

本研究では、大気中のスス粒子の変質と粒子形態との関係および雲・降水過程によるエアロゾル粒子の優勢集団の変遷を理解するため、1）大気中を長距離輸送されたスス含有粒子の形態と水溶性物質量、および、2）スス粒子の吸湿性の有無と雲・降水過程による外部混合状態の変化との関係を明らかにすることを目的とする。そこで、1）、2）の目的に応じた二つの観測を実施した。エアロゾル粒子の粒子形態は透過型電子顕微鏡を用いて調べた。ススは水に不溶性の物質であり、数十 nm の小球が鎖状に連なった特有の形態を有する。水溶性物質の抽出（水透析）前後の電子顕微鏡写真の比較により、個々の粒子中のススの有無と水不溶性物質/水溶性物質の体積比を調べた。電子顕微鏡観察の試料採取に役立てるため、直径 0.1～0.5 μm のエアロゾル粒子の個数濃度と粒径別のススの質量濃度とを測定した。さらに、エアロゾル粒子の吸湿性の指標として、乾燥時の直径が 0.5 μm 以下で、加湿後も直径が小さい粒子（相対湿度 88％で直径 0.56 μm 以下の粒子、以下 less-grown（LG）粒子と呼ぶ）の数濃度を測定した。

排出源からの輸送中に変質したスス含有粒子の粒子形態の特徴を明らかにするため、中国からの風下にあたる沖縄・辺戸岬において2008年3月に観測を行なった。辺戸岬では、後方流跡線解析とエアロゾル濃度に基づき、黄海西岸地域の中国から 1～5 日かけて輸送された気塊について、6 つの試料を選び、粒子（0.2～0.7 μm）を分析した。中国由来の気塊中のススの質量濃度は、直径<0.3 μm よりも>0.3 μm の粒径範囲で高い傾向にあった。水透析法と電子顕微鏡観察によれば、スス含有粒子の数割合は直径 0.2～0.4 μm の粒子で 2～25%、0.4～0.7 μm で 14～59%であった。 ほとんどのススが水溶性物質との混合粒子として観察された。個々のス

ス含有粒子に含まれる水溶性物質の体積割合は、どの試料でも中央値が 80%以上であり、ス ス含有粒子の大部分が水溶性物質であることが示唆された。エネルギー分散型 X 線分析計で 個別粒子を分析した結果とエアロゾル質量分析計の結果によれば、水溶性物質は主に SO_4^{2-}と 有機物、NH_4^+であることが示唆された。主たる組成として NH_4HSO_4 が示唆された試料では、サ イズによる粒子形態の違いは見られなかった。試料採取時の湿度は NH_4HSO_4 の潮解湿度より 高かったため、粒子は大気中で液体であったと考えられる。一方、主たる組成として$(NH_4)_2SO_4$ が示唆された試料では、スス含有粒子の形態は、粒径区分ごとに異なった。直径 0.4 μm 以下で は球体粒子、0.4 μm 以上では約 0.3 μm の球体が複数個連結した形態の粒子の割合が高かっ た。球体粒子と連結型粒子を構成する球体のサイズおよび形態は類似していた。試料採取時 の湿度は、$(NH_4)_2SO_4$ の潮解湿度よりも低く、粒子は大気中で固体として存在していたと考えら れる。そのため、球体粒子が凝集することにより連結型粒子が形成された可能性が考えられる。 直径 0.3 μm の粒子の凝集による連結型粒子の形成について検討するため、簡単な凝集モデ ルにより中国からの輸送時間内に形成される凝集粒子の数濃度を見積もった。その結果は、北 京などの大都市で観測されるような粒子数濃度が高い場合であれば、凝集過程によって連結 型粒子が形成される可能性があることを示唆した。

スス粒子の変質の有無と雲・降水過程による外部混合状態の変化との関係を調べるために、 雲・降水過程を経ても大気に残る可能性の高い、雲の中のエアロゾル粒子（雲粒間粒子）の吸 湿性をスス含有粒子に注目して調べた。観測は、2007 年 6 月に標高 2300 m の立山・天狗平に 行なった。霧粒間のエアロゾル粒子を調べるため、試料の取り込み口で 10 μm 以上の粒子を除 去した後の粒子を測定した。霧の発生時、粒子数濃度は 1～2 桁低い値を示した。降水強度が 強い（2～6 mm/hr）霧の発生時、乾燥直径 0.3～0.5 μm の LG 粒子の数割合は約 100%を示 した。ススの質量濃度のほとんどは直径 0.4 μm 以下の粒子によるもので、0.1～0.5 μm の粒子体 積に占める 0.4 μm 以下の粒子によるスス体積割合は高い値（70%）を示した。電子顕微鏡観察 用に採取した LG 粒子の試料について水透析した結果では、0.1～0.5 μm の粒子の約 9 割が水 不溶性であり、その半分以上が鎖状のススであった。そのため、雲粒間粒子の多くが水溶性物 質の付着していないスス粒子であった事が示唆された。一方、降水強度の弱い（約 1 mm/hr） 霧の発生時には、LG 粒子の数割合は低く（50%）、0.1～0.5 μm の粒子体積に占める 0.4 μm 以 下のスス体積割合は 20%以下であった。LG 粒子の試料において、水溶性物質を含有する粒 子が多く、雲粒間粒子の多くが吸湿性粒子であった事が示唆された。また、ススと水溶性物質 の混合粒子も観察された。これらの結果から、降水を伴う雲の形成条件に応じて、水溶性物質 を含んだスス含有粒子も雲粒間粒子として存在し得るが、強い降水を伴う雲内では、水溶性物 質の付着していないスス粒子が優先的に雲粒間に残ることが示唆された。

本研究では、野外観測と電子顕微鏡観察下での実験による結果から、大気中のスス含有粒 子のサイズ、水溶性物質の付着量、および粒子形態を変える要因について議論した。本研究 で得られた結果を総合すると、従来から知られている低揮発性物質の凝縮に加えて、高い粒 子数濃度下では凝集による変質がスス含有粒子の形態的特徴を変えること、雲・降水時 にはスス粒子の外部混合状態が変わることが示唆された。

Abstract

Soot in atmospheric aerosol particles is dominant absorber of visible solar radiation in the atmosphere. Soot particles are emitted into the atmosphere mainly by fossil fuel combustion and biomass burning. Although soot particles freshly emitted by fossil fuel combustion are submicron and mostly hydrophobic, atmospheric aging process can modify soot particles to hydrophilic particles that are internally mixed soot with water-soluble materials. Atmospheric aging processes of aerosol particles include adsorption and condensation of semi-volatile vapors, coagulation of particles with other preexisting aerosol particles, and adsorption into droplet particles under humid conditions in the atmosphere. The estimation of spatial distribution and light absorbing and scattering amounts of soot-containing particles are essential to evaluate climate effect of soot in the atmosphere. The optical properties of soot-containing particles depend on volume of the other materials on soot and morphology of soot-containing particles. Because the optical properties of soot-containing particles can be altered in the atmosphere by atmospheric aging processes, it is important to understand modification process of morphological features of soot-containing particles during transport in the atmosphere. However, morphology and mixing volume of soluble materials of atmospheric soot-containing particles has little been studied at a same time; relations between aging and morphology of soot-containing particles are not fully understood. On the other hand, transport amounts of soot-containing particles to remote area are influenced by scavenging processes during transport. For submicron soot-containing particles, in-cloud scavenging processes including scavenging into cloud droplets and precipitation acts as the major removal process from the atmosphere. Cloud-forming potentials of a submicron particle largely depend on hygroscopicity of the particle. Although cloud-forming potentials of soot particles can be enhanced by mixing with soluble materials, fresh hydrophobic soot particles have low cloud-forming potentials and might have less chance to be removed by rain drops. The knowledge of mixing states of hydrophobic soot particles and hygroscopic soot-containing particles in cloud interstitial air is important for quality and quantity of soot-containing particles after in-cloud scavenging process.

This study elucidates 1) morphology and internal mixing states with soluble materials of soot-containing particles after transport, and 2) modification of external mixing states between hydrophobic and hygroscopic soot-containing particles by in-cloud scavenging. Two observations were made for the objectives. Morphological features of individual particles were analyzed by using a transmission electron microscopy (TEM). Soot is insoluble and has a characteristic structure like a chain or chain aggregation of primary spherules having diameter of about 20–50 nm. Mixing states with soot, and volume of water-soluble materials in individual particles were analyzed by comparison between microscopic photographs before and after dialysis (extraction) of water-soluble materials (water dialysis). Size-segregated soot mass concentrations and number concentrations of dried particles (0.1–0.5 μm diameter) selected for less-grown (LG) particles (particles smaller than 0.56 μm diameter at 88% relative humidity) were measured to monitor quantify hygroscopic tendencies of aerosol particles.

To elucidate morphological changes after aging of soot-containing particles during transport from the major source area, atmospheric observations for East Asian outflow were made at Cape Hedo, Okinawa, Japan in March 2008. Based on the backward air trajectory analysis, six aerosol samples collected in air masses from similar source regions (central eastern China) with different speed (1–5 days) to the site were analyzed for particles of 0.2–0.7 μm in diameter. Soot mass concentration of >0.3 μm particles tended to be higher than that of <0.3 μm during air mass derived from China. Based on the TEM analysis with water dialysis, number proportions of soot-containing particles to total particles for 0.4–0.7 μm (14–59%) were higher than that for 0.2–0.4 μm (2–25%). Median values of volume ratio of soluble materials in individual soot-containing particles for each sample were larger than 80% for all samples, suggesting that most volume of soot-containing particles were water soluble materials. Results of energy dispersive X-ray analysis on individual particles and aerosol chemical measurements at the site suggested that soluble materials in the samples mainly consisted of SO_4^{2-}, organics and NH_4^+. For samples suggested that dominant component was NH_4HSO_4, the morphological features of particles did not show clear dependency on the particle size. Because relative humidity of outside air during the sampling period was higher than

deliquescence humidity of NH_4HSO_4, most aerosol particles existed as liquid droplets in the atmosphere. For samples suggested that dominant component was $(NH_4)_2SO_4$, most soot-containing particles were spheroid for 0.2–0.4 μm, and clustered shape connecting multiple small (ca. 0.3 μm diameter) units for larger size range (0.4–0.7 μm). The shape and size of a unit of cluster-like particles were similar to that of spheroidal particles. Because relative humidity of outside air during the sampling period was lower than deliquescence humidity of $(NH_4)_2SO_4$, most aerosol particles existed as solid particles in the atmosphere. These features of soot-containing particles implied formation of clustered particles by coagulation process. To investigate the possibility of formation of coagulation cluster, the number concentration of coagulated particles were estimated using a simple coagulation model with initial unit diameter of 0.3 μm during transport time. The results suggested that sufficient number of coagulation clusters can be formed under high aerosol number concentration that is comparable with that in the Beijing.

To study relation between in-cloud scavenging and modification of external mixing states of hydrophobic and hygroscopic soot-containing particles, the observation for cloud interstitial particles was made at Mt. Tateyama, Japan (2300 m a.s.l.) in June 2007. Aerosol particles were measured using fog (>10 μm)-cut inlets to select cloud interstitial particles. During fog conditions, the aerosol (>0.3 μm diameter) number concentration decreased about 1–2 orders of magnitude. During fog condition under high precipitation (2–6 mm/hr), number fractions of the LG particles to total particles of 0.3–0.5 μm were nearly 100%. Volume fraction of soot (<0.4 μm) to aerosols (0.1–0.5 μm) were high values (ca. 70%). For TEM sample, most particles (0.1–0.5 μm) were water insoluble. More than half of the water-insoluble particles were considered to be soot particles showing chain-aggregations, suggesting that most cloud interstitial particles were soot particles without water-soluble materials. During fog condition under low precipitation (ca. 1 mm/hr), number fractions of the LG particles of 0.3–0.5 μm were low (ca. 50%) and volume fraction of soot (<0.4 μm) to aerosols (0.1–0.5 μm) were lower than 20%. For TEM samples of LG particles, most particles were partly water soluble, suggesting that most cloud interstitial particles were hygroscopic particles. Partly soluble materials containing soot were also found in the samples. The results at Mt. Tateyama suggested

that soot-containing particles internally mixed with soluble materials can exist as cloud interstitial particles according to the meteorological condition, but soot particles without soluble materials are preferentially left behind as interstitial particles in cloud with high precipitation.

Based on the observation results of morphology and mixing states of soot-containing particles, this study discussed about the internal and external changes of the soot-containing particles in the atmosphere. In addition to condensation process known already, modification with coagulation process under high aerosol concentration and population change of the particles with in-cloud scavenging process are suggested as key processes controlling size, volume of soluble materials and morphological features of soot-containing particles in the atmosphere.

Contents

1. Introduction

1.1. Sources and climatic effects of soot particles in the atmosphere

Atmospheric aerosol particles play an important role in estimating climate effects by directly scattering and absorbing solar radiation while acting indirectly as cloud condensation nuclei (CCN) [e.g. *Twomey*, 1977; *Pilinis et al.*, 1995; *Haywood and Boucher*, 2000]. Atmospheric aerosol particles comprise water-soluble (sea salts, nitrate, sulfate, etc.) and water-insoluble (silicate minerals, soot, etc.) materials [e.g. *Seinfeld and Pandi*s, 2006]. Among these components, soot is a dominant absorber of visible solar radiation in the atmosphere. Soot is a byproduct of the combustion and consists of elemental carbon (EC) and organic carbon (OC) [e.g. *Seinfeld and Pandis*, 2006]. Light absorbing part of soot is called black carbon (BC) which is almost the same as EC. According to report of Intergovernmental Panel on Climate Change at 2007, some major aerosol species cause negative forcing (the estimates of direct effects are: sulfate, -0.4 [±0.2] W/m^2; fossil fuel OC, -0.05 [±0.05] W/m^2; nitrate, -0.1 [±0.1] W/m^2; and mineral dust, -0.1 [±0.2] W/m^2), and total radiative forcing of aerosols was estimated to be also negative (direct forcing, -0.50 [±0.40] W/m^2; and indirect forcing, -0.70 [-1.1, +0.4] W/m^2). However, soot-containing aerosols (fossil fuel BC and biomass burning aerosols) influence radiative forcing positively (respectively, +0.2 [±0.15] and +0.03 [±0.12] W/m^2 for direct effect) because of light absorption of BC.

Atmospheric soot is emitted largely from fossil fuel combustion (diesel and coal), open biomass burning (associated with deforestation and crop residue burning), and cooking with biofuels [*Ramanathan and Carmichael*, 2008]. Globally, the annual emissions of BC are (for the year 1996) ~8 Tg yr^{-1}, with about 20% from biofuels, 40% from fossil fuels and 40% from open biomass burning [*Bond et al.,* 2004]. Table 1-1 lists emissions of BC from fuel combustion (fossil and biofuel combustion and excludes

open burning) and from open biomass burning [*Bond et al.*, 2004]. Based on the Table 1-1, emissions of BC from fuel combustion were especially high in China and India, and that from open biomass burning was high in Central/South America and Africa. About half of the world total soot emission from fuel combustion was originated from Asia. Figure 1-1 presents global distribution of BC sources by *Bond et al.,* [2004]. High BC emissions occur in both the northern (largely from fossil fuel combustion) and the Southern (largely from open burning) Hemispheres. Although North America and Western Europe seemed to be the major sources of soot emissions until about the 1950s, now developing nations in the tropics and East Asia are the major source regions [*Novakov et al.*, 2003; *Bond et al.*, 2007]. Recent East Asian economic development engenders considerable enhancement of anthropogenic emissions of not only soot, but also SO_2, NO_x, organic carbon etc [*Streets et al.,* 2003; *Ohara et al.*, 2007].

Soot in atmospheric aerosol particles can strongly enhance global and regional radiative forcing of the atmosphere [e.g. *Haywood and Boucher*, 2000; *Chung et al.*, 2005; *Ramanathan and Carmichael*, 2008]. Figure 1-2 presents global distribution of BC radiative forcing that is obtained from integration of satellite aerosol data, surface network of aerosol remote sensing instruments and field observations with an aerosol-transport-chemical model and a radiative transfer model by *Chung et al.* [2005]. The uncertainty in the forcing is ±30%. The peaks of the BC radiative forcing are close to major source regions and give rise to regional hotspots of atmospheric solar heating due to BC. The high radiative forcing regions spread around the major source regions. Some studies have also reported for brown clouds around the hotspots, which generally denote anthropogenic aerosols strongly scatter and absorb solar radiation due to soot and other species [e.g. *Ramanathan et al.*, 2007; *Nakajima et al.*, 2007].

On the other hand, resent studies suggested that the soot engender warming effect not

Table 1-1. Emissions of Black Carbon[a] compiled by *Bond et al.* [2004]

Region	From Fuel Combustion[b]		From Open Burning	
	Central	(Low-High)	Central	(Low-High)
North America[c]	382	(278–618)	116	(49–494)
Central/South America	360	(254–791)	910	(487–2581)
Europe	466	(339–841)	59	(29–229)
Former USSR	178	(135–524)	100	(44–416)
China	1365	(863–3395)	124	(72–282)
India	483	(307–1035)	92	(49–224)
Other Asia	727	(528–1457)	275	(127–896)
Pacific	32	(23–52)	165	(75–469)
Africa	477	(297–1000)	1472	(675–4223)
Middle East	156	(107–372)	11	(6–29)
Total	4626	(3132–10,084)	3325	(1614–9842)

[a]Units are Gg/yr.
[b]"Fuel Combustion" includes fossil and biofuel combustion and excludes open burning.
[c]North America includes Canada, the United States, and Mexico.

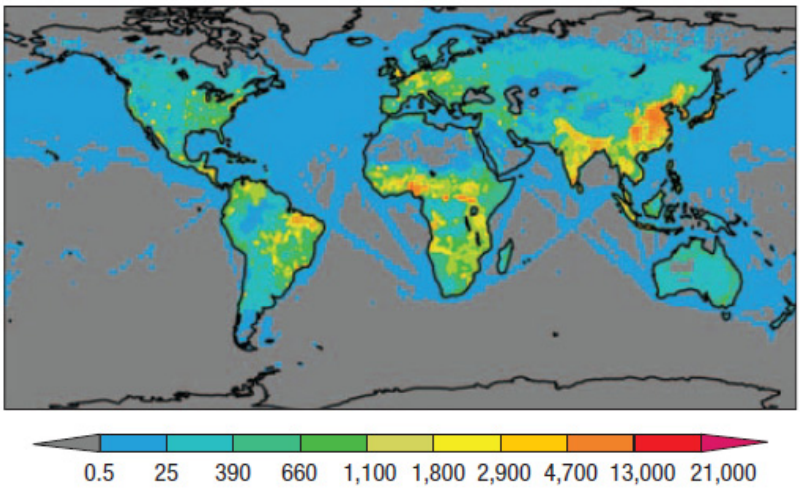

Figure 1-1 Global distribution of BC sources. The BC emission strength in tons per year from a study by *Bond et al.*[2004], including emissions from fuel combustion (fossil fuels and biofuels) and open biomass burning (forest fires, savanna burning and outdoor cooking) for the year 1996. The uncertainty in the regional emission is about ±100% or more. This figure is cited from *Ramanathan and Carmichael* [2008].

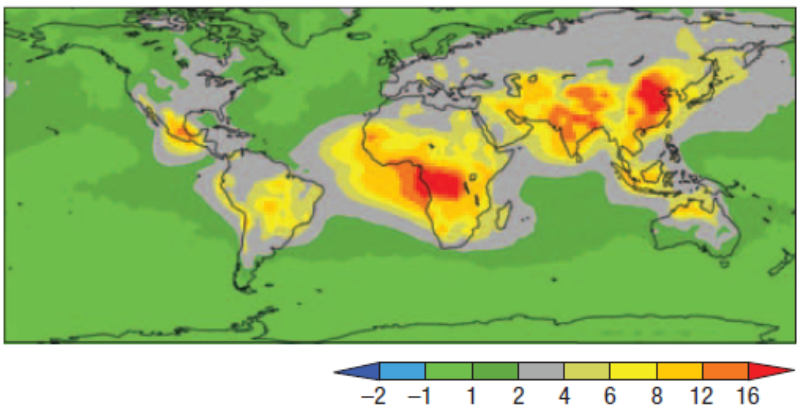

Figure 1-2 Global distribution of BC radiative forcing. Atmospheric solar heating due to BC from the study by *Chung et al*. [2005] for the 2001 to 2003 period. This study integrates satellite aerosol data, surface network of aerosol remote sensing instruments and field observations with an aerosol-transport-chemical model and a radiative transfer model to obtain the forcing. Uncertainty in the forcing is ±30%. This figure is cited from *Ramanathan and Carmichael* [2008].

only through the atmosphere but also through positive feedback on snow and ice albedo after the long-range transport and deposition on the snow albedo at mid-to-high latitudes [*Hansen and Nazarenco*, 2004; *Koch and Hansen*, 2005; *Ramanathan and Carmichael*, 2008]. This indirect soot forcing through the snow surface includes the trends thinning Arctic sea ice, and melting land ice and permafrost. *Hansen and Nazarenco* [2004] reported that plausible estimates for the effect of soot on snow and ice albedos in the Arctic and Northern Hemisphere land areas yield a climate forcing of -0.3 W/m^2 in the Northern Hemisphere. The estimated effects on snow and ice albedos were not negligible level for global radiative forcing. Because emission of soot in the Arctic is small, large part of soot in snow and ice are considered to be transported from polluted distant area. According to a simulation study using a global model by *Koch and Hansen* [2005], they suggested that the surface BC concentrations in the Arctic is attributed to transport with 25% from Europe, 24% from Russia, 20% from Asia, 16% from biomass burning (including northern and southern hemispheres), and 14% from North America. However, because soot is notoriously difficult to simulate spatial distribution, they have also noted that their model tended to underestimate about BC concentrations near source regions and overestimate the concentrations in more remote regions.

Many studies have been suggested that atmospheric soot influences climate forcing. Especially, huge amount of anthropogenic soot emitted from major source regions could largely affect on global warming even after long-range transported. To evaluate climate forcing due to soot in the atmosphere, it needs to be simulated spatial distribution after transportation and the light absorbing amount by soot. However, the current estimates of soot effects still include large uncertainties. One of the important causes of estimation uncertainties is the mixing states of the soot-containing particles with the other aerosol components. Soot-containing particles in the atmosphere exist as two main types of

mixing states: a soot particle without the other components (external mixture) and a soot-containing particle mixed with the other components within a particle (internal mixture). In this study, soot particles with and without the other components are referred to collectively as soot-containing particles. Internal mixture of soot has many various states, such as volume and compositions of the other materials. The mixing states of soot-containing particles can be modified in the atmosphere with atmospheric aging process and wet scavenging process. The atmospheric aging process and wet scavenging process of aerosol particles will be explained in the following sections 1.2 and 1.3 respectively. Assuming different mixing states of soot-containing particles lead to diversity of the spatial distributions and the absorbing effect of soot in the atmosphere [e.g. *Haywood et al.*, 1997; *Jacobson*, 2001; *Croft et al.*, 2005; *Stier et al.*, 2006; *Adachi et al.*, 2010; *Lack and Cappa*, 2010]. In addition to changes in mixing states of soot-containing particles, changes in morphological features of the particles have also been increasingly investigated to estimate their optical properties [*Khalizov et al.*, 2009a; *Adachi et al.*, 2010]. *Adachi et al.* [2010] investigated morphological factors of internally mixed soot-containing particles at Mexico City using electron microscopy, and estimated the optical property from the morphological factor and chemical components. They applied the obtained optical property to climate model and reported that the contribution to direct radiative forcing assuming a non-spherical soot particle embedded by sulfate and organic matters was ca. 20% less than if soot particle had a simple core shell shape. Although the optical and physicochemical properties of soot-containing particles are essential parameters to evaluate climate forcing, they can be modified with changes of the morphology and the mixing state. Therefore, it is important to understand modification of morphology and mixing states of soot-containing particles in the atmosphere.

1.2. Atmospheric aging processes and modification of soot particles

Atmospheric aging processes of aerosol particles include adsorption and condensation of semi-volatile vapors, coagulation of particles with other preexisting aerosol particles, heterogeneous reactions at the particle surface with gaseous species, and in-cloud processing in the atmosphere [*Fuchs*, 1964; *Husar and Whitby*, 1973; *Mamane and Gottlieb*, 1989; *Meng and Seinfeld*, 1994]. In-cloud process consists of growth into cloud droplet, adsorption of soluble species and aqueous reaction, and evaporation [*Meng and Seinfeld*, 1994]. Growth processes of a particle by condensation of gaseous species, heterogeneous reactions, and in-cloud processing are all related to the addition of new aerosol materials. The efficiency of particle growth due to aging processes depends on various conditions including size distribution, aerosol and the precursor gas concentrations and meteorological conditions.

Soot particles freshly emitted by fossil fuels burning are mostly hydrophobic [*Weingartner et al.*, 1997; *Zuberi et al.*, 2005] and largely distribute in submicron size range [*Huang and Yu*, 2006]. However, the soot particles can be modified to hydrophilic particles that are internally mixed soot with water-soluble materials by atmospheric aging process. The aging processes of soot particles also alter their morphologies and mixing volumes with soluble materials, and eventually changing their optical properties of soot-containing particles [*Fuller et al.*, 1999; *Bond and Bergstrom*, 2006; *Worringen et al.*, 2008; *Khalizov et al.*, 2009a]. Changes in mixing state of soot-containing particles resulting from heterogeneous condensation have been studied using laboratory experiments [*Kahalizov et al.*, 2009a, 2009b; *Pagels et al.*, 2009]. *Kahalizov et al.* [2009a and 2009b] reported that condensation of sulfuric acid on soot particles altered the particle size and morphology, and that it enhanced hygroscopicity and light absorbing and scattering of the soot particles. Furthermore, increase of size and

hygroscopicity of soot-containing particles by aging process enhance the ability of acting as cloud condensation nuclei of the particle, enhancing the possibility to be removed by wet scavenging, and eventually reducing atmospheric residence time of the particles [*Andreae and Rosenfeld*, 2008].

As previous studies have suggested, morphology and mixing states of soot-containing particles are important factors to estimate light absorbing effect of atmospheric soot. However, the morphology and mixing states of soot-containing particles can be modified with atmospheric aging processes, in accordance with various conditions. Therefore, modification of atmospheric soot-containing particles must be understood. However, there are few observation data of morphological features with mixing states.

1.3. Modification of mixing states after wet scavenging process

Light absorbing property of soot-containing particles can affect on climate change at remote area after long-range transport from source area, as explained in section 1-1. Transport amount of soot-containing particles to remote area is largely reduced by atmospheric wet scavenging process during transport. Some numerical sensitivity studies have examined aging and wet scavenging parameters of soot in the atmosphere properly to simulate long-range transport and spatial distributions of soot-containing particles in the atmosphere [*Ogren and Charlson*, 1983; *Koch*, 2001; *Croft et al.*, 2005; *Stier et al.*, 2006].

Wet scavenging consists of below-cloud and in-cloud scavenging processes according to the location of aerosol inclusion. For below-cloud scavenging processes, collision efficiency with rain droplet depends on the size of particles and rain droplets,

and intensity of rain [*Slinn*, 1983]. The below-cloud scavenging process can efficiently remove particles of larger than 2 μm in diameter. However, the collision between rain droplets and particles of 0.1–1 μm in diameter is not efficient. Therefore, submicron soot-containing particles are not removed easily by below-cloud scavenging process unless after grown to lager than 1 μm by aging process. On the other hand, in-cloud scavenging processes include nucleation to cloud droplets and impaction and diffusion of aerosol particles to cloud droplets within clouds. After particles growing into cloud droplets, rain drops efficiently scavenge the cloud droplets [*Pruppacher and Klett*, 1997]. Therefore, especially for sub-micrometer particles, in-cloud scavenging acts as the major removal process from the atmosphere to the earth's surface.

On the other hand, cloud-forming potential of a submicron particle largely depend on size and hygroscopicity of the particle. The cloud-forming potentials of soot particles can be enhanced by mixing with soluble materials. However, fresh hydrophobic soot particles have low cloud-forming potentials. Therefore they might be left behind after nucleation scavenging. Because such aerosol particles left behind after nucleation scavenging have less chance to be collected by rain drops, the cloud interstitial particles might have some higher likelihood of surviving longer in the atmosphere: they will therefore have a higher probability of being transported longer distances. The knowledge of mixing states of hydrophobic soot particles and hygroscopic soot-containing particles in cloud interstitial air is important to consider amount and light absorbing effect of soot-containing particles after in-cloud scavenging process. However, the mixing states of cloud interstitial particles in the atmosphere remain poor understanding.

Relating to scavenging process, *Naoe and Okada* [2001] observed individual soot-containing particles at Tsukuba using electron microscopic analysis of samples

before and after water dialysis. They reported that soot particles without water-soluble material were abundant during rainfall events, probably because of the scavenging of soot-containing internally mixed with soluble materials by rain. However, the report was based on ground-level observations, conducted far below the clouds. Therefore, they cannot provide information related to particles in cloud interstitial air aloft. Scavenging efficiencies of soot particles growing into cloud droplets have been observed at high elevation sites under fog conditions [*Hallberg et al.*, 1992, 1994; *Kasper-Giebl et al.*, 2000; *Hitzenberger et al.*, 2000, 2001; *Acker et al.*, 2002; *Cozic et al.*, 2007]. According to review for the soot mass scavenging efficiencies into cloud droplets by *Cozic, et al* [2007], the scavenging efficiencies at rural locations tended to be lower than those in urban locations, implying differences in cloud-forming ability of soot-containing particles. On the other hand, the scavenging efficiencies of soot also showed variations according to cloud-forming conditions, such as temperature and liquid water content [*Kasper-Giebl et al.*, 2000; *Hitzenberger et al.*, 2001; *Cozic et al*., 2007]. Based on individual analyses of particles in the interstitial air and cloud droplets at Mt. Kleiner Feldberg, *Hallberg et al.* [1994] reported that most particles forming cloud droplets were soluble, whereas insoluble particles and few soluble particles remained in the interstitial air. The proportion between insoluble soot particles and hygroscopic particles might also be modified according to cloud-forming condition. However, details of the mixing states were not described with the prevailing meteorological conditions in the previous reports.

1.4. Morphology of soot particles and advantages in microscopic analysis

The morphology of soot in the atmosphere is often studied using Transmission Electron Microscopy (TEM) and Scanning Electron Microscopy (SEM). Soot is

recognizable by its special morphology by scanning or transmission electron microscopy [e.g. *Janzen*, 1980; *Gelencser*, 2004; *Pósfai et al.*, 2004; *Murr and Soto*, 2005]. Figure 1-3 shows an electron micrograph of soot particles collected at the road side near Nagoya University. Soot particles have often ramified and apparently irregular agglomerate structure that consisted of primary spherules having diameter of about 20–50 nm, which is like a chain or chain aggregation. In addition to morphological feature, data on mixing state of water-soluble and -insoluble materials of a particle can also be obtained using an electron microscopy and water dialysis analysis [*Okada*, 1983]. Figure 1-4 shows electron micrographs before and after water dialysis of soot particles collected at Nagoya. Because soot is water insoluble, chain-like shaped soot remain on film after water dialysis. Chain-like particle A did not show morphological change after water dialysis. On the other hand, shape of chain-like particle B partly changed after water dialysis, suggesting the particle is soot-containing particle internally mixed with water-soluble materials. Several studies of the mixing state of soot-containing aerosols have also been conducted using water dialysis [*Naoe and Okada*, 2001; *Okada and Hitzenberger*, 2001; *Hasegawa and Ohta*, 2002]. Furthermore, *Okada* [1983] developed a method to estimate volume of soluble materials in a particle using microscopic analysis with water dialysis.

There are some methods that can also provide information of mixing states of particles. Mixing states between hydrophobic and hygroscopic particles were measured by Hygroscopic Tandem Differential Mobility Analyzer [e.g. *Liu et al.*, 1978; *Swietlicki et al*., 2008]. However, the methods do not provide information for soot inclusion in particles. On the other hand, mixing states of soot-containing particles were measured using a single-particle soot photometer [e.g. *Moteki et al.*, 2007; *Schwarz et al.*, 2008]. This instrument provides information of coating thickness of soot particles, but does not

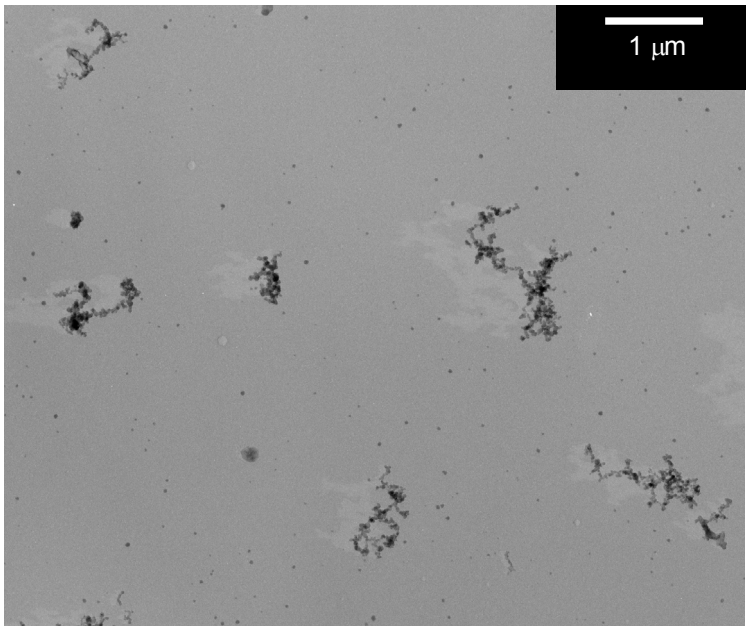

Figure 1-3 Electron micrographs of soot particles at the road side.

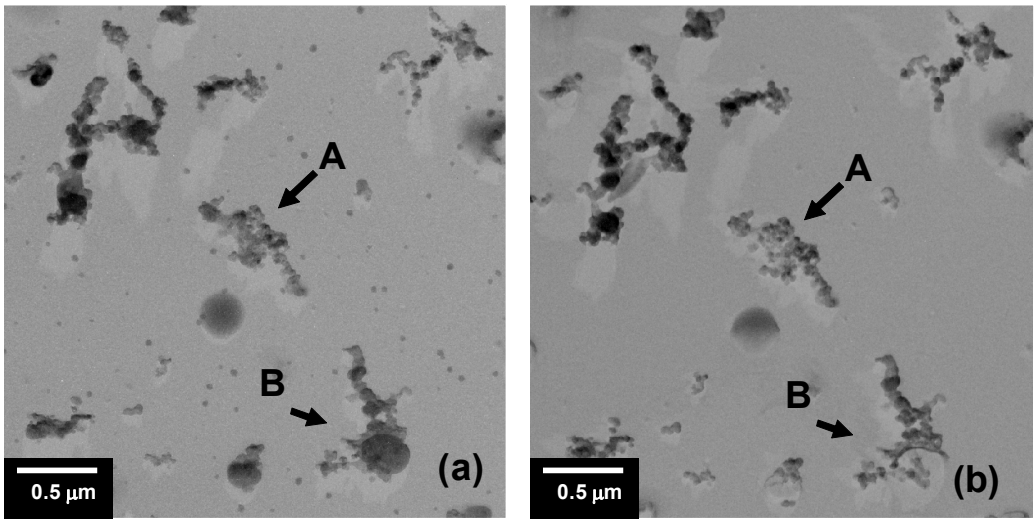

Figure 1-4 Electron micrographs before (a) and after (b) water dialysis of particles collected at Nagoya.

inform particle morphology and type of mixed or coated materials. Although microscopic analysis is time-consuming and labor-intensive work comparing to the other methods, the microscopic analysis with water dialysis can only provide detailed information of morphological features of individual particles including mixing states with soluble materials.

1.5. Objective of this study

This study is designed for better understanding about modification processes of morphological features and mixing states with soluble materials of soot-containing particles during transport, focusing on aging and in-cloud scavenging processes. This study elucidates 1) morphology and mixing states with soluble materials of soot-containing particles after transport, and 2) modification of mixing states between hydrophobic and hygroscopic soot-containing particles by in-cloud scavenging. Two observations were made for the objectives respectively. In this study, morphological types of aerosol particles and mixing states of soot particles with water-soluble materials were classified by using an electron microscope analysis with water dialysis method [*Okada*, 1983]. Microscopic analysis is time-consuming and labor-intensive work. Moreover, it cannot provide data showing continuous and real-time mixing state variations. In this study, an index of the diameter growth factors or hygroscopicities of aerosol particles of 0.3–0.5 μm diameter was produced using a new continuous monitoring system to optimize the sampling strategy of representative aerosol samples for studying the mixing states.

As explained in section 1.1., anthropogenic soot emitted from major source area can affect on climate forcing not only near the source area but also the leeward areas after

long-range transport. The soot-containing particles are transported probably with changing their physicochemical and optical properties of the particles due to modification of the morphology and mixing states. At first, to understand modification of morphology and mixing state in the atmosphere, this study elucidates morphological features of soot-containing particles in continental outflow from East Asia, as the aging consequence of soot particles from the major source region. For collecting aerosols in continental outflow, atmospheric observation was made at Cape Hedo, Okinawa, Japan. Chapter 3 presents the results at Cape Hedo and discusses about relation between morphological features of soot-containing particles and aging processes during transport. On the other hand, as explained in section 1.3, external mixing states between hydrophobic and hygroscopic soot-containing particles can be modified after in-cloud scavenging process. The change of population and mixing states of soot-containing particles by in-cloud process is important to consider transport amount and optical property of soot-containing particles after in-cloud scavenging process. As a second objective, this study elucidates the modifications of mixing states between hydrophobic and hygroscopic soot-containing particles of cloud interstitial particles. To investigate fog interstitial particles as surviving after in-cloud scavenging, atmospheric observation was conducted at a high-elevation site, Tengudaira (2300 m a.s.l.) of Mt. Tateyama. Chapter 4 presents the results at Mt. Tateyama focusing on the mixing state of the fog interstitial particles with respect to soot. Finally, in addition to previous knowledge, changing process of morphology and mixing states of soot-containing particles in the life cycle are discussed with new results of two observations in Chapter 5.

2. Measurements and laboratory methods

2.1. Number–size distribution of aerosol particles and size segregated soot mass concentration

The number–size distribution of atmospheric particles was measured using a laser particle counter (KC-18; Rion Co. Ltd.). The laser particle counter (LPC) measures the number concentrations of aerosol particles for five size ranges: diameters greater than 0.1, 0.15, 0.2, 0.3, and 0.5 μm. The aerosol measurements were made at relative humidity (RH) of 15–25% monitored in line using the data logger (MR6600; Chino Corp.).

The mass concentration of soot particles was measured using a particle soot absorption photometer (PSAP; Radiance Research), as derived from the particle light absorption coefficient at a 565 nm wavelength. To obtain size information related to soot particles, two impactors (nozzle diameters 0.7 and 1.2 mm, flow rates 1.6 and 2.0 $l \cdot min^{-1}$, respectively at Mt. Tateyama, and nozzle diameters 0.4 and 1.2 mm, flow rates 0.8 and 1.0 $l \cdot min^{-1}$, respectively at Cape Hedo) and two two-way valves were used to cut particles larger than the cut off diameters (0.4 and 1.1 μm at Mt. Tateyama and 0.3 and 1.6 μm at Cape Hedo). The valves were changed every 6–20 min with integration time of 1–5 min for one soot datum. The soot mass concentration was calculated from the measured absorption coefficient by assuming a specific absorption of 10 $m^2 \cdot g^{-1}$ [*Hansen et al.*, 1984; *Gelencsér*, 2004]. The volume concentration of soot particles was estimated assuming a density of 1.8 $g \cdot cm^{-3}$ for soot [*Janzen*, 1980].

2.2. Continuous monitoring of aerosol hygroscopicity for a selected size range

As an index of diameter growth factor or hygroscopicity of the 0.3–0.5-μm-diameter

aerosol particle population, the number ratios of less-grown (LG) particles (particles smaller than 0.56 μm after humidifying at 88% RH) to total particles of 0.3−0.5 μm dried diameter were monitored continuously at the site. Because of instrumental limitations of the LPC and impactors, this size range represented the best choice to measure the diameter growth factor of atmospheric aerosol particles. A schematic diagram of the monitoring system is presented in Fig. 2-1. After removal of large particles (>3 μm at Cape Hedo and >10 μm diameter at Mt. Tateyama) at the inlet, the sample air was introduced to the room (about 20°C) and humidified at 88±3% RH. The RH sensors were calibrated, respectively, at 75 and 83% RH using saturated solutions of NaCl and Na_2SO_4. At this RH, hygroscopic particles might increase their diameter depending on their chemical composition. For example, the respective diameter growth factors of ammonium sulfate, ammonium nitrate, and sodium chloride are 1.67, 1.7, and 2.28 at 88% RH [*Tang and Munkelwitz*, 1993]. Next, the sample air was introduced to line A or B. At the front of the LPC inlet, lines A and B were switched every 20 min through the two two-way valves using a time controller. Lines A and B respectively provide number concentrations of LG particles and total particles of 0.1−0.5 μm diameter. In line A, the >0.56 μm diameter particles that had become larger under the humid condition were cut by an impactor. For example, the impactor respectively removes particles having diameter growth factors >1.87 and >1.12 for 0.3 and 0.5 μm diameter. Then the remaining particles were counted by the LPC after drying in a diffusion dryer at 15–25%RH. The number concentration of the remaining particles is designated as the number concentration of LG particles: N_{LG}. Line B provides a particle number concentration for particles <0.56 μm in diameter at 15–25%RH, which is defined as the number concentration of total particles for a given size range (0.3−0.5 μm diameter): N_T. The aerodynamic 50% cut off diameter (d_{50}) was estimated for 1 atm or 850 hPa at 2300

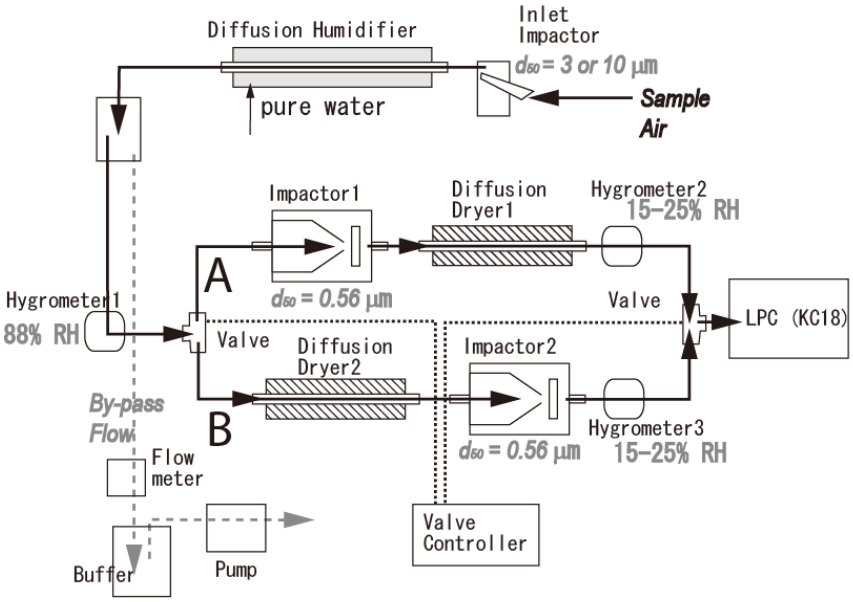

Figure 2-1 Flow diagram of a measurement system for less-grown (LG) particles (particles smaller than 0.56 μm diameter at 88% relative humidity) and total aerosol particles. Black arrow lines and gray dotted arrows respectively indicate flow lines of sample air and by-path flows.

m.a.s.l.at Tateyama [*Hinds*, 1999]. As an index of the abundance of LG particles, the number fraction of LG particles of 0.3–0.5 μm (F_{LG}) was calculated using the following equation.

$$F_{\mathrm{LG}} = \frac{N_{LG,0.3-0.5}}{N_{T,0.3-0.5}} \times 100 \ [\%] \tag{2-1}$$

The F_{LG} value depends on the diameter growth factors of individual particles and the number size distribution of the particles with diameters of 0.3–0.5 μm. Figure 2-2 shows the estimated F_{LG} values as a function of various mixing types and volume fractions of water-insoluble cores with soluble materials in the particle population. The F_{LG} values were estimated by assuming the following. 1) Aerosol particles consist of external or internal mixtures between water-insoluble (non-hygroscopic) and water-soluble materials such as ammonium sulfate (major component of fine aerosol particles observed in this study). 2) The mixing state and volume fraction of insoluble materials is uniform in the diameter range of 0.3–0.5 μm. 3) The number size distribution follows a simple power law distribution of aerosol particles known as Junge's distribution [*Junge*, 1963], given as

$$\frac{dN}{d\log D} = \alpha D^{-\beta}, \tag{2-2}$$

where D, N, α, and β respectively stand for the particle diameter, number concentration of particle with diameter D, a constant, and a slope of the size distribution. Here we respectively assigned 3 and 6 to β according to observed slopes of number size

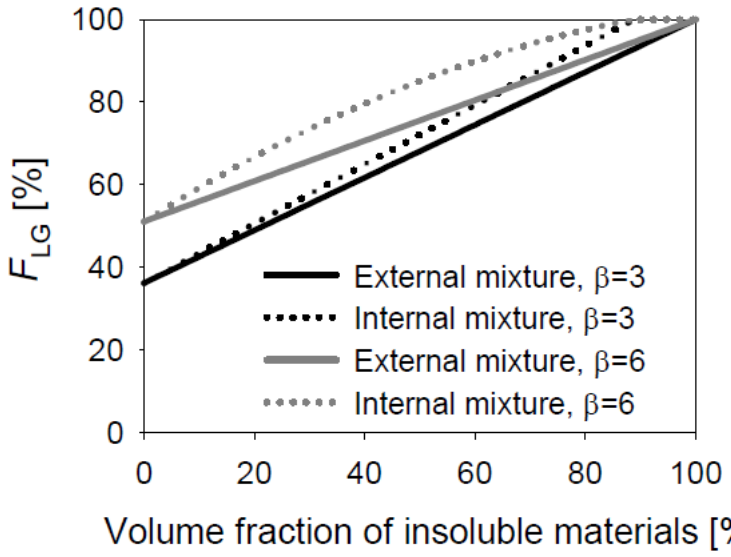

Figure 2-2 Relation between volume fraction of water-insoluble materials and fraction of LG particles for 0.3–0.5 μm in diameter (F_{LG}, see the text). The F_{LG} were calculated by assuming a mixing state (external or internal mixture) and a slope of size distribution β.

distributions between 0.2–0.3 μm and 0.3–0.5 μm during usual and foggy conditions. All F_{LG} values in Fig. 2-2 increase concomitantly with the increasing volume fraction of insoluble materials. Although β and mixing states alter F_{LG}, differences of the F_{LG} values are within 20% for the same volume fraction of insoluble materials. It is noteworthy that the measured F_{LG} does not provide the diameter growth factor itself. In general, measurements of the diameter growth factor have been performed using narrow size ranges of particles [e.g., *Swietlickli et al*., 1999; 2008]. In these reports of the literature, less-hygrosocopic and more-hygroscopicic particles represent particles having the diameter growth factors of 1.1–1.15 and 1.38–1.69, respectively at 90% RH. However, our parameter, F_{LG}, is useful to quantify "the tendency of growth characteristics" for an aerosol population in a given size range, as depicted in Fig. 2-2. Unlike complicated measurement of the diameter growth factors by Hygroscopic Tandem Differential Mobility Analyzer, the F_{LG} can be monitored in-situ conveniently and continuously. Therefore, the F_{LG} of 0.3–0.5 μm diameter was used to decide the aerosol sampling strategy at the site.

2.3. Individual particle analysis

Aerosol particles and less-grown particles were collected to study morphological analysis using a transmission electron microscope (TEM). To analyze morphological feature of aerosol particles, dried (relative humidity <20%) aerosols were collected by cascade impactors (50% cut of diameters of the three stages, respectively, 0.5 μm, 0.3 μm, and 0.2 μm) on carbon-coated nitrocellulose (collodion) films. The sampling system of LG particles, which is depicted in Fig. 2-3, is similar to line A in Fig. 2-1, but a second impactor is attached to collect particles (d_{50} of the first and second impactors were,

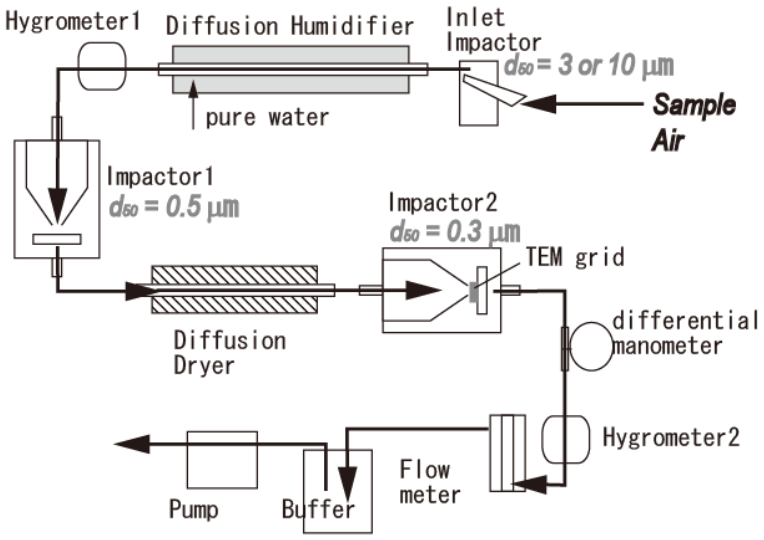

Figure 2-3 Flow diagram of sampling line for LG particles. Black arrows indicate paths of sample air.

respectively, 0.5 μm and 0.3 μm) instead of the LPC after the diffusion dryer, particles were collected in the second impactor. These samples were stored under dry conditions at room temperature until TEM analyses performed at Nagoya University and the Meteorological Research Institute.

Particles collected on the carbon film were photographed using transmission electron microscopes (H600; Hitachi Ltd. and JEM-2010; JEOL) at 2000× magnification. To measure the height of individual particles on the collection surface, particles were coated with a Pt/Pd alloy at a shadowing angle of 26.6° (arctan 0.5). The Pt/Pd coating thickness was about 7 Å. The collection film is regarded as a semipermeable membrane. Therefore, a water dialysis technique [*Mossop*, 1963; *Okada*, 1983; *Okada et al.*, 2001] was applied to aerosol samples to remove water-soluble materials from the individual aerosol particles through the film. The aerosol sample on the electron microscopic grid was floated on ultrapure water at 40°C for 3 hr with the collection side upward (see Figs. 4a and 4c in *Okada et al.* [2001]). The water-insoluble residues after dialysis were coated again perpendicularly to the previous coat of a Pt/Pd alloy to differentiate the particle height and two-dimensional morphology after water dialysis.

The negative films were scanned and recorded with a resolution of 1200 dpi. The scanned image was processed using image analysis software (Win Roof; Mitani Corp.) to estimate the projected area of a particle (S). Shadow lengths (l) of individual particles were measured manually. The sphere-equivalent diameter of each particle was calculated from measurements of S and l according to the method described in *Okada* [1983]. The mixing states of individual particles with respect to water solubility were obtained by comparing the electron micrographs of the same field of the collecting surface taken before and after water dialysis.

Figure 2-4 presents examples of electron micrographs of the same particles taken

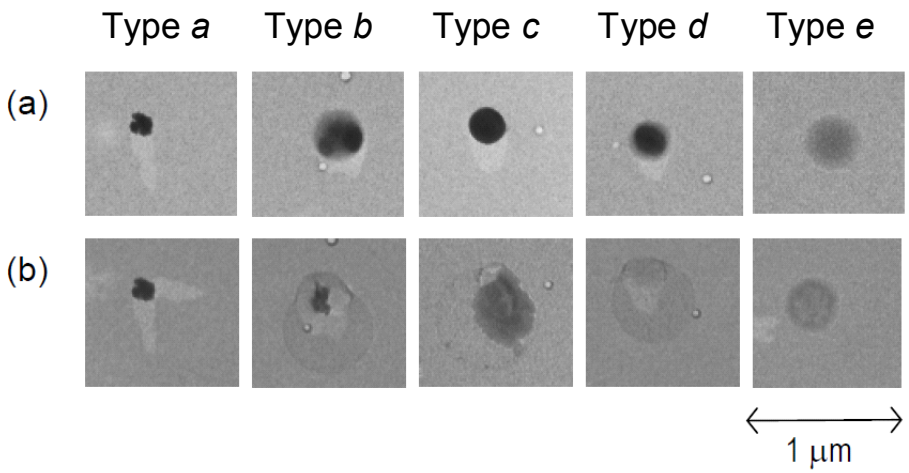

Figure 2-4 Electron micrographs of the same individual particles before (row a) and after dialysis with water (row b): Type *a*, insoluble particle; Type *b*, mixed particle (insoluble core with soluble material); Type *d*, completely soluble particle; Type *c*, intermediate morphology between Type *b* and Type *d*; and Type *e*, other than Types *a*–*d* with semi-transparent particles without apparent change after water dialysis.

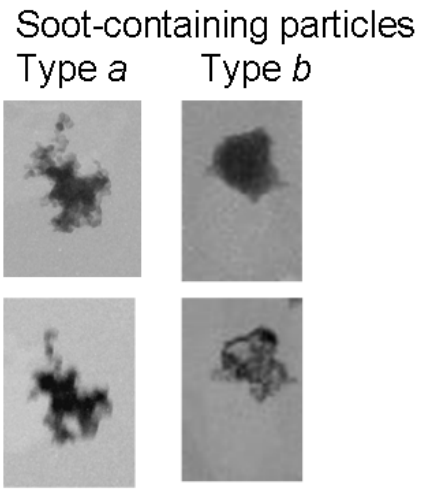

Figure 2-5 Electron micrographs of the same individual soot-containing particles of Types *a* and *b* before (row a) and after dialysis with water (row b)

before and after water dialysis. Particles were classified into five types, as in the process described by *Naoe and Okada* [2001]. Type *a* includes water-insoluble particles showing no change in morphological appearance before and after dialysis. Type *b* includes mixed particles composed of water-soluble and water-insoluble materials. Type *d* includes soluble particles without water-insoluble inclusions. Type *c* comprises particles having intermediate appearance between those of Type *b* and Type *d*, showing a partly water-soluble appearance, but not having an apparent water-insoluble core. Particles of Type *e* show a semi-transparent appearance in the electron beam and show no apparent change in morphology by dialysis. Particles of this type might be composed mainly of organic materials [*Okada et al.*, 2001]. For some particles of Types *a* and *b*, insoluble materials in the particles were often aggregation shape of globules less than 50 nm in diameter like particles shown in Figure 2-5. Such aggregations were often considered as soot particles [*Janzen*, 1980; *Pósfai et al.*, 2004; *Murr and Soto*, 2005]. In this study, Types *a* and *b* particles having soot-like-shaped insoluble materials are collectively called soot-containing particles.

Crystal structural information was obtained for some particles using selected-area electron diffraction (SAED) before water dialysis. In addition, the elemental compositions of some residual particles after dialysis were analyzed using an energy-dispersive X-ray (EDX) analyzer (EMAX-5770X; Horiba Ltd.) equipped with a scanning electron microscope (SEM, DS-I30C; Topcon Corp.) at Nagoya University.

2.4. Chemical constituents of aerosol particles

At Cape Hedo Aerosol and Atmospheric Monitoring Station (CHAAMS) in Okinawa, chemical constituents of aerosols were measured by an Aerodyne quadruple

aerosol mass spectrometer (Q-AMS; Aerodyne Research, Inc., MA) which was capable to monitor non-refractory chemical components (NO_3^-, SO_4^{2-}, Cl^-, NH_4^+ and organics) of aerosol particles < 1μm in diameter [*Takami et al.*, 2007]. During our observation period, >90% of the measured materials were comprised of SO_4^{2-}, NH_4^+ and organics by mass.

In observation at Mt. Tateyama, for chemical analysis, size-segregated aerosol particles were collected using a two-stage stacked filter pack (47 mm diameter, NILU) placed in a plastic weather shield having an open window at the bottom facing downward. Aerosol particles were collected using a Nuclepore polycarbonate filter (8 μm pore size; Nomura Micro Science Co. Ltd.) at the first stage and a Teflon membrane filter (nominal pore size 1.0 μm diameter; J100A047; Advantec Toyo Kaisha Ltd.) at the second stage, at a flow rate of ca. 12 $l \cdot min^{-1}$. After sampling, each filter was stored in a polypropylene 15 ml centrifuge vial with an airtight cap (Iwaki Glass Co. Ltd.). Each was kept in a freezer until laboratory analyses. To extract water-soluble components from the aerosol particles, 10 ml of ultrapure water (18MΩ, Milli-Q water; Millipore Corp.) was added. Details of the ionic chemical and pH analyses were described in *Osada et al.* [2007]. The analyzed ions were Cl^-, NO_3^-, SO_4^{2-}, NO_2^-, Br^-, PO_4^{3-}, CH_3COO^-, $HCOO^-$, $CH_3SO_3^-$, and $C_2O_4^{2-}$ (anions), and H^+, Na^+, NH_4^+, K^+, Mg^{2+}, and Ca^{2+} (cations). Procedural blank samples were treated identically to actual aerosol samples. Concentrations of procedural blank samples were mostly negligible. However, any concentration found was subtracted from the value in the actual sample.

2.5. Backward air trajectory

Backward air mass trajectory was computed using the Hybrid Single-Particle Lagrangian Integrated Trajectory (HYSPLIT) model developed by NOAA ARL

[*Draxler and Rolph*, 2003; *Rolph*, 2003]. The National Weather Service's National Centers for Environmental Prediction (NCEP) FNL archive was used for meteorological input data. Precipitation intensities along trajectory pathway were used.

3. Morphological features of soot-containing particles in the continental outflow observed at Cape Hedo, Okinawa

Resent study suggested that the soot particles emitted from anthropogenic source engender warming effect not only at the source area but also the leeward areas after long-range transport. In particular, East Asian economic development in recent years engenders considerable enhancement of anthropogenic emissions of soot, SO_2, NO_x, organic carbon etc [*Streets et al.,* 2003; *Ohara et al.*, 2007]. The huge amount of soot and the other aerosols emitted from East Asia has been transported to leeward area, such as north Pacific [*Kaneyasu and Murayama*, 2000]. In this study, to elucidate the aging consequence of morphological feature and mixing state of soot-containing particles after transport from the East China, soot-containing particles were observed at Cape Hedo, Okinawa, Japan, as a leeward site of the huge emission source. This chapter presents observation results at Cape Hedo and discuss about changing processes of morphological feature and mixing states of soot particles during transport.

3.1. Atmospheric observation at Cape Hedo

Atmospheric observations were conducted at Cape Hedo, Okinawa, Japan (26.87°N, 128.25°E, 60 m asl) during March 19–30 in 2008. Figure 3-1 portrays a location map of the observation site of Cape Hedo. The Cape Hedo Aerosol and Atmospheric Monitoring Station (CHAAMS) is located at the north end of Okinawa Island. The site is located about 100 km distant from populated areas of southern Okinawa Island. In previous studies, CHAAMS has been used to study the outflow of air pollution from eastern Asia (Takami et al., 2007; Takiguchi et al., 2008). Various parameters have been monitored at the site such as meteorological data (temperature, humidity, precipitation,

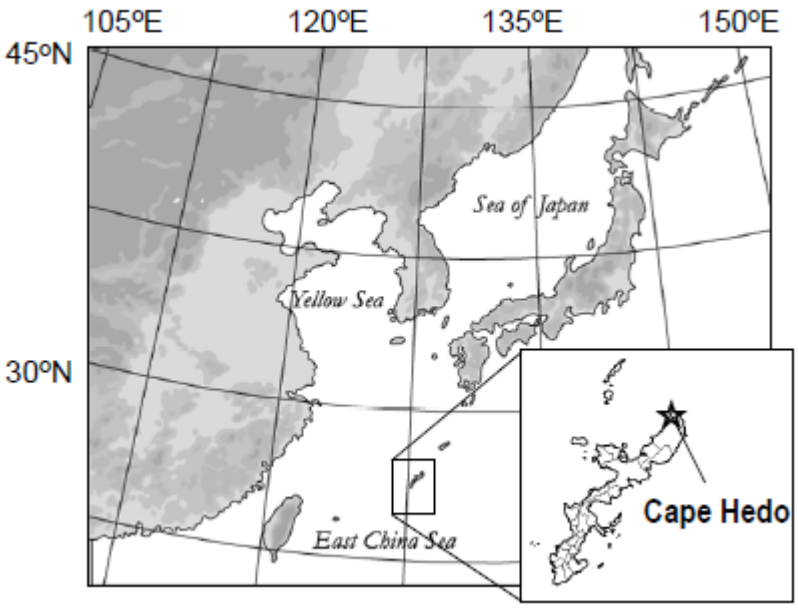

Figure 3-1 Location of Cape Hedo, Okinawa, Japan.

wind speed direction etc.), concentrations of gaseous species (SO_2 CO, NOx, O_3, etc.), and physical and chemical parameters of aerosol particles (http://www.nies.go.jp/asia/hedomisaki/outline_e.html).

An aerosol measurements and sampling systems were set in a room at CHAAMS. The inlets were placed on the roof about 3 m above the ground. To remove coarse aerosol particles, impactors having aerodynamic 50% cut off diameter of 3 μm were used at the inlet for measurement and sampling lines.

3.2. Backward air trajectory and sample selection for TEM analysis

Among the many TEM samples taken, six samples were selected according to differences in aerosol concentration and backward air trajectories of air mass derived from almost identical source area in eastern central China. Table 3-1 presents sampling details of the TEM samples discussed in this study, size-segregated aerosol and soot concentrations, chemical data obtained using Q-AMS, and SO_2 concentrations. Figure 3-2 portrays 120 hr horizontal backward air trajectories for samples A–F. The backward trajectory data were computed using the Hybrid Single-Particle Lagrangian Integrated Trajectory (HYSPLIT 4) model developed by the National Oceanic and Atmospheric Administration (NOAA) Air Resources Laboratory (ARL) [*Draxler and Rolph*, 2003; *Rolph*, 2003]. The horizontal air trajectory suggested that the air masses for all samples (A–F) were transported to the site across the East China Sea from the Shandong area in China. Transport durations from the coast of China to the sampling site were respectively, 19, 22, 32 47, 82 and 113 hr for samples A, B, C, D, E, and F.

Table 3-1 Sampling period of TEM samples A–F, ambient air condition, number concentration, soot-mass concentration, soot mass-size ratio, chemical data obtained by Q-AMS, and SO_2 concentrations.

Sample ID	**A**	**B**	**C**	**D**	**E**	**F**
Sampling date (2008)	23-Mar	24-Mar	24-Mar	26-Mar	27-Mar	28-Mar
start	21:01	8:54	14:38	16:08	6:06	9:20
stop	21:26	9:04	14:53	16:23	6:16	9:38
Ambient air						
Temperature [°C]	18.3	17.2	18.6	18.9	18.3	19.8
Relative Humidity [%]	71	58	53	62	67	−
Number conc. [#/cm^3]						
0.1-0.2 μm	399	955	508	917	510	1171
0.2-0.3 μm	92	470	185	336	227	566
0.3-0.5 μm	18	205	76	103	64	216
Soot mass conc. of <1.6 μm [μg/m^3]	2.5	18.6	4.7	12.5	7.6	25.0
Soot mass ratio of <0.3/<1.6 μm	0.38	0.18	0.26	0.09	0.06	0.08
Q-AMS (particle<1 μm)						
Mass conc. [μg/m^3]						
NH_4^+	0.5	4.9	3.1	4.8	3.3	6.2
SO_4^{2-}	3.2	9.5	15.6	11.2	9.3	13.3
Org.	1.4	4.8	4.8	5.3	3.9	7.5
Total mass of NH_4^++SO_4^{2-} +NO_3^-+Cl^-+Org.	5.2	20.3	23.7	21.6	16.7	27.4
Molar ratio of						
NH_4^+/SO_4^{2-}	0.85	2.72	1.06	2.28	1.91	2.47
$NH_4^+/(SO_4^{2-}+NO_3^-+Cl^-)$	0.81	2.30	1.04	2.23	1.84	2.35
SO_2 conc. [ppb]*	0.1	2.5	1.4	2.8	1.2	4.1

*: Data from Ministry of the Environment and Asia Center for Air Pollution Research (http://www.acap.asia/index.html).

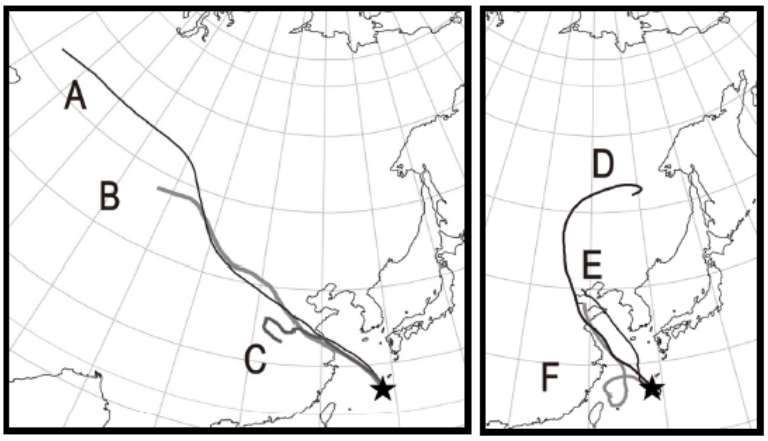

Figure 3-2 120 hr horizontal backward trajectories for samples A−F. Trajectories were calculated from altitudes at 500 m a.s.l.

3.3. Temporal variations of aerosol volume and size segregated soot-mass concentrations

Figure 3-3 temporal variations in meteorological parameters and aerosol properties observed during 19–30 March 2008. Figure 3-3a presents air temperature, relative humidity and 10 min precipitation intensity at this site. Meteorological data at Cape Hedo from 18:00 on 27th to 10:30 on 28 March (indicated as horizontal bar in Fig. 3-3a) were unavailable. For this period, data of temperature, precipitation and wind were substituted from a meteorological observatory at Oku located 5 km southeast of Cape Hedo (http://www.jma.go.jp/jma/index.html). Precipitation was observed on 23 and 30 March, the other days were fine or cloudy conditions. A cold front passed over the site at 14:00 on 23 March. Figure 3-3b presents wind speed and direction data. Figure 3-3c indicates potential source areas of air masses according to backward air trajectories. During nights on 23–30 March, air masses originated mainly from China. Figure 3-3d presents volume concentrations (0.1−0.5 μm in diameter) of aerosol particles with indications of samples (A–F) for TEM analysis. Aerosol data are presented after screening by local wind direction (clockwise, SSE to WSW) from populated areas of Okinawa Island. The volume concentrations (0.1−0.5 μm in diameter) were calculated from number concentrations for each size range of the LPC and their geometric mean diameters assuming spherical particles. The volume concentrations were mostly lower than 5 $\mu m^3/cm^3$, but often increased to higher than 10 $\mu m^3/cm^3$. High aerosol concentration events were observed on the morning of 24 March, the afternoon of 26 March, and the morning of 28 March, corresponding respectively to samples B, D, and F (Fig. 3-3d). However, aerosol concentrations were moderate for samples A, C, and E.

Figure 3-3e shows size-segregated soot-mass concentrations in aerosols. Soot mass concentrations of <1.6 μm varied in phase with aerosol volume concentration of

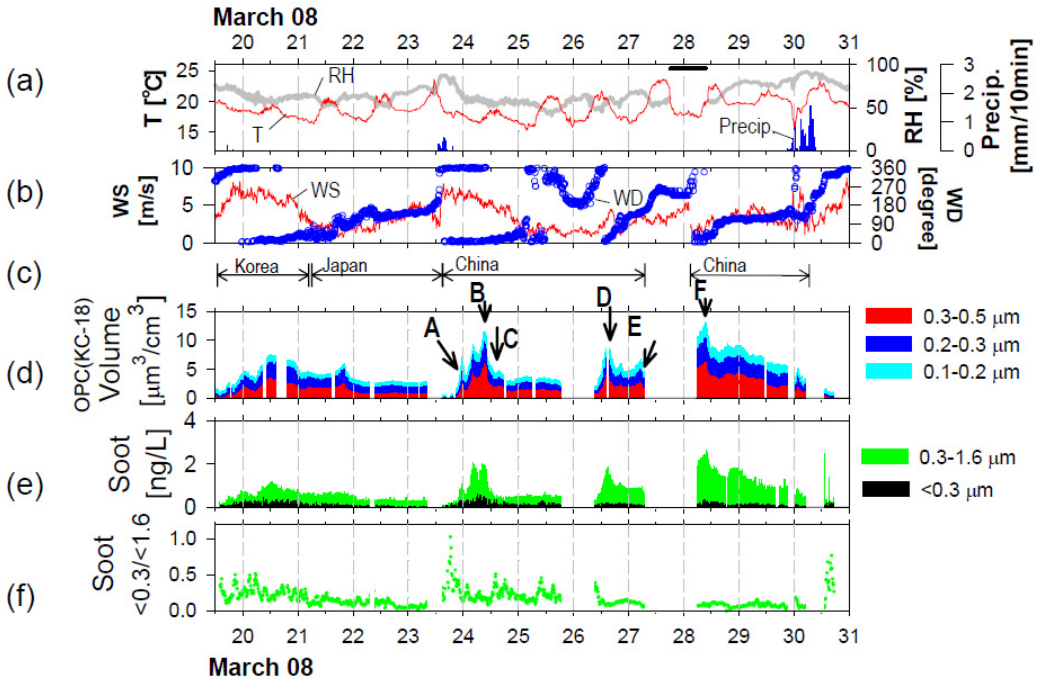

Figure3-3 Temporal variations of (a) temperature, relative humidity and precipitation, (b) wind speed and direction, (c) air mass origin, (d) volume concentrations of aerosols for 0.1−0.5 μm in diameter and sampling times (A–F with arrows), (e) size segregated soot mass concentration, (f) soot mass–size ratio of <0.3 μm to <1.6 μm. The horizontal black bar in (a) represents duration of lack of meteorological data at the site.

0.1−0.5μm in diameter. Assuming the soot density as 1.8 g cm^{-3} [*Janzen*, 1980], estimated volume ratio of soot (<1.6 μm) to volume concentration of particles (0.1–0.5μm diameter) were less than 0.2 during most of the observation period. Figure 3-3f presents mass–size ratio of <0.3 μm to <1.6 μm diameter soot-containing particles. The soot mass–size ratio were 0.0–1.0, but the values were mostly less than 0.2, indicating that about 80% of soot-containing particles existed as larger than 0.3 μm in diameter. Among TEM samples, soot mass–size ratios (<0.3 μm /<1.6 μm) for samples A, B and C were higher than about 0.2 (Table 3-1). Based on the backward trajectory analysis, the transport time after leaving the Chinese coast was about 1 day for these samples; the soot size-mass ratios (<0.3 μm /<1.6 μm) were lower than 0.1 for remainder of the samples (D, E and F) which took more than 2 days from the Chinese coast. The relation between soot mass–size ratios and transport time after source areas implies that the size of soot-containing particles increases after emission.

Although continuous soot size monitoring was limited for only two channels, detailed size distribution of light absorption coefficient were obtained for 18:08–19:14 on 28 March, immediately after sample F was taken, as portrayed in Fig. 3-4. The size distribution using 7 channels was obtained by manually the changing flow rates and impactors having different cut-off diameters. A bimodal size distribution was found for this period with a valley at 0.4–0.5 μm and peaks at 0.3–0.4 μm and 0.5–0.6 μm in diameter. Similar bimodal size distributions for soot-containing particles have been reported at some urban sites (Los Angeles in the US, *Venkataraman and Friedlander*, 1994; Uji in Japan, *Hitzenberger and Tohno*, 2001; South China, *Huang and Yu*, 2008). Based on the diameter of a valley shown in Fig. 3-4, morphological features of particles will be presented separately at 0.4 μm in the following sections.

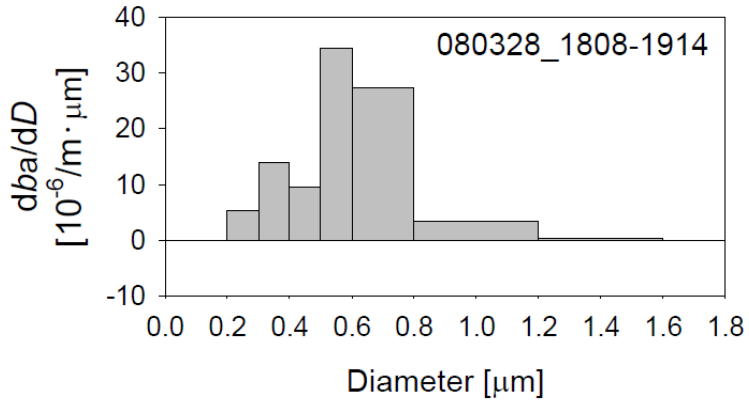

Figure3-4 Size distribution of light absorption coefficient on 28 March.

3.4. Morphological types of individual aerosol particles

Morphological features of aerosol particles in this study were classified into six types, as presented in Figure 3-5. Particle classified as Type 1 is an aggregation of globules less than 50 nm in diameter. Such aggregations were often regarded as soot particles [*Janzen*, 1980; *Pósfai et al.*, 2004; *Murr and Soto*, 2005]. Based on results of EDX analysis, Types 1 particles showed considerably high carbon peak intensity compared with the background spectra of the collodion film. Type 2 is a single spheroidal particle showing strong contrast to the film and longer Pt/Pd shadow than the particle diameter with a characteristic shadow shape. Type 2 particle were rich in sulfur according to result of EDX analysis. According to Q-AMS results, Type 2 particles were found dominantly on samples collected when the molar ratio of NH_4^+/SO_4^{2-} was greater than two (0:00–10:30 on 24 March, 15:30 on 26–4:00 on 27 March, and during 6:00 on 28 – 14:30 on 29 March), suggesting existence of ammonium sulfate ($(NH_4)_2SO_4$) and other ammonium salts. Furthermore, SAED analysis of Type 2 particles showed some faint spots matching with that of $(NH_4)_2SO_4$, implying that spheroidal particles partly comprised amorphous materials: they were not pure crystal of $(NH_4)_2SO_4$. Type 3 are cocoon-shaped particles that are characterized as having parallel straight lines for the particle perimeter. The aspect ratios of parallel straight line length to perpendicular length of the particles were 1–4. Based on the EDX analysis, Type 3 particle was also rich in sulfur. The SAED results of Type 3 particles showed clear pattern of $(NH_4)_2SO_4$, indicating that the particle had crystal structure of ammonium sulfate. Sulfur-rich particles having a similar cocoon-shaped shape were also reported from several studies of aerosols derived from biomass burning and urban sources [*Li et al.*, 2003; *Li and Shao*, 2010]. Type 4 shows weak contrast to the collection film and a short Pt/Pd shadow. Because of the short shadow length, the height of the Type 4 particle is low, implying

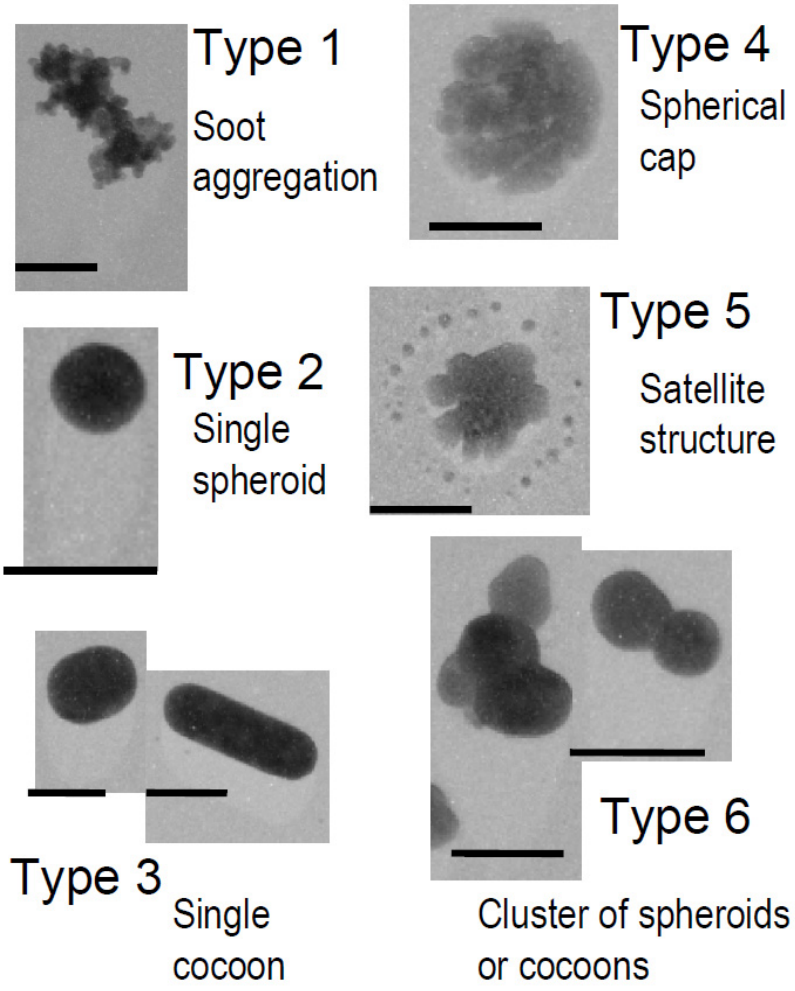

Figure 3-5 Morphological classification types 1–6 of particles. Horizontal bars in photographs represent length of 0.5 μm.

shape of spherical cap [*Okada*, 1983]. Type 4 particle were rich in sulfur according to result of EDX analysis. Particles of Type 5 have smaller satellite particles aligned as a ring around the center particle: a so-called the satellite structure. The central particle in the satellite structure usually had short length of a Pt/Pd shadow, which was similar to that of a Type 4 particle. The satellite stricture has been found to occur often in sulfuric acid droplets [*Gras and Ayers*, 1979; *Bigg*, 1980; *Ferek et al.*, 1983]. Reports describe that the shape of the satellite ring correlated with the degree of ammonization, such as single ring of satellites for bisulfate (NH_4HSO_4) as the central particle. In this study, satellite ring of Type 5 particles was usually single. Indeed, the molar ratios of NH_4^+/SO_4^{2-} in fine aerosols were close to unity (20:20–21:30 on 23 March and 12:30–19:00 on 24 March) when Type 5 particles were found in TEM samples, suggesting that ammonium bisulfate (NH_4HSO_4) was the dominant compound. Type 6 are clustered particles connected to form many spheroidal or cocoon-shaped units resembling Type 2 and 3 particles for shape and size (0.2–0.5 μm in diameter) in the same sample. Particles of Type 6 comprised 2–10 (sometimes more than 20) units of Type 2 or 3 particles. Type 6 particles were also rich in sulfur, as revealed by EDX analysis.

Figure 3-6 portrays size-segregated number proportions of morphological types of particles for samples A–F, based on classification of Fig. 3-5. Size patterns of morphological types for the samples show two groups: 1) combinations of Type 4 (spherical caps) and Type 5 (satellite structure) particles, irrespective of size as found in samples A and C; and 2) combinations of Type 2 (spheroidal) or Type 3 (cocoon-shaped) for a smaller size range (0.2–0.4 μm) and Type 6 (clustered) for a larger size range (0.4–0.7 μm diameter) as found in samples B, D, E, and F. The number of connected units in a particle of Type 6 for 0.4–0.7 μm diameter was 2–10 units with the average of

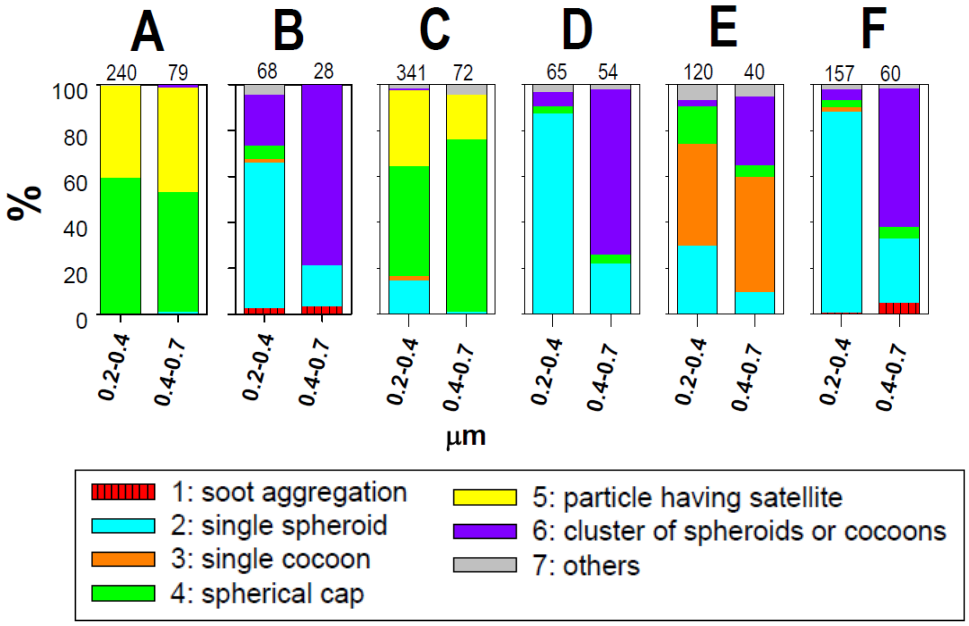

Figure 3-6 Number proportions of morphological types of particles for samples A–F. Classification of morphological types 1–6 are the same as in Fig. 3-5. Numbers above columns indicate the numbers of particles observed.

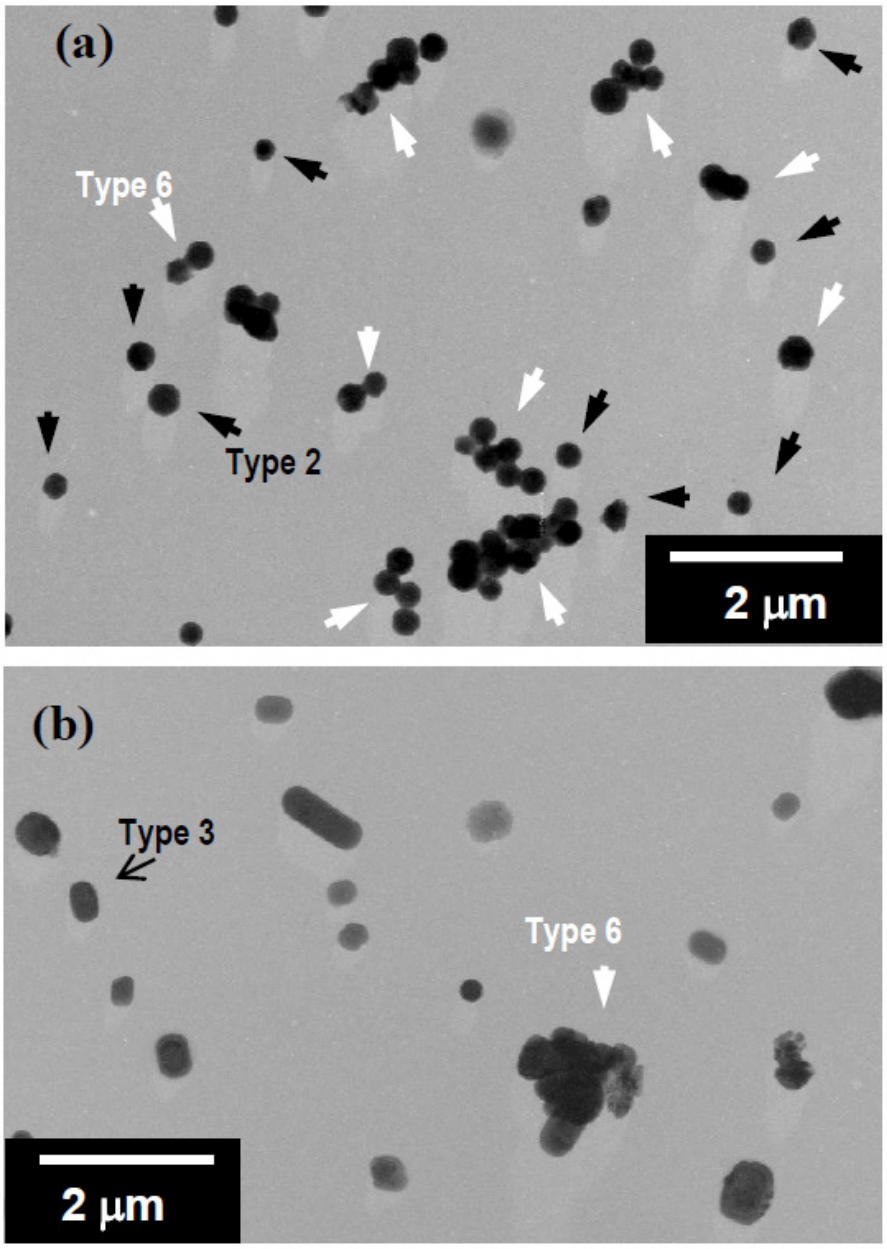

Figure 3-7 Examples of electron micrographs for samples D (a) and E (b). White, black and thin black arrows respectively indicate Type 6, 2 and 3 particles.

2.2–3.8 units for samples B, D, E and F. As an example of Type 6 particles, TEM images of samples D and E are shown respectively, in Figure 3-7a and 3-7b. Type 6 particles with spheroidal units are indicated by white arrows on sample D in Fig. 3-7a. The size and shape of spheroidal units in a cluster resembled those of Type 2 (black-arrow-indicated) particles on the same samples. Type 6 particles of samples B and F resembled those of sample D described here. However, Type 6 particles on sample E in Fig. 3-7b were composed mainly of cocoon-like units that resembled Type 3 particles on the same sample.

3.5. Mixing states and morphological features of soot-containing particles

Figure 3-8 shows morphological differences between Type 1–6 particles before (a, b, c and d) and after (a', b', c' and d') water dialysis. Images of (a'), (b'), (c') and (d') were taken for the same region at the same magnification as (a), (b), (c) and (d) respectively. Based on a comparison of differences between images taken before and after dialysis, particles of Types 2–6 were found to be mostly water soluble. Most Type 1 particles showed no morphological change after water dialysis, or showed a slightly collapsed shape like that in Fig. 3-8c' after dialysis. Some Type 2–6 particles also contained insoluble cores having a characteristic shape of soot (black arrows in Fig. 3-8a' and d'). Although soot protruding at the particle fringe was recognized in some cases before water dialysis (as indicated by a black arrow in Fig. 3-8d), >80% of the soot in Type 2, 3 and 6 particles was found in particles as completely coated by soluble materials (e.g. particle indicated by a black arrow in Fig. 3-8a).

Number proportions of the mixing state types of particles based on water dialysis are presented in Fig. 3-9 for samples A–F. Insoluble soot particle (Type *a*) were quite rare

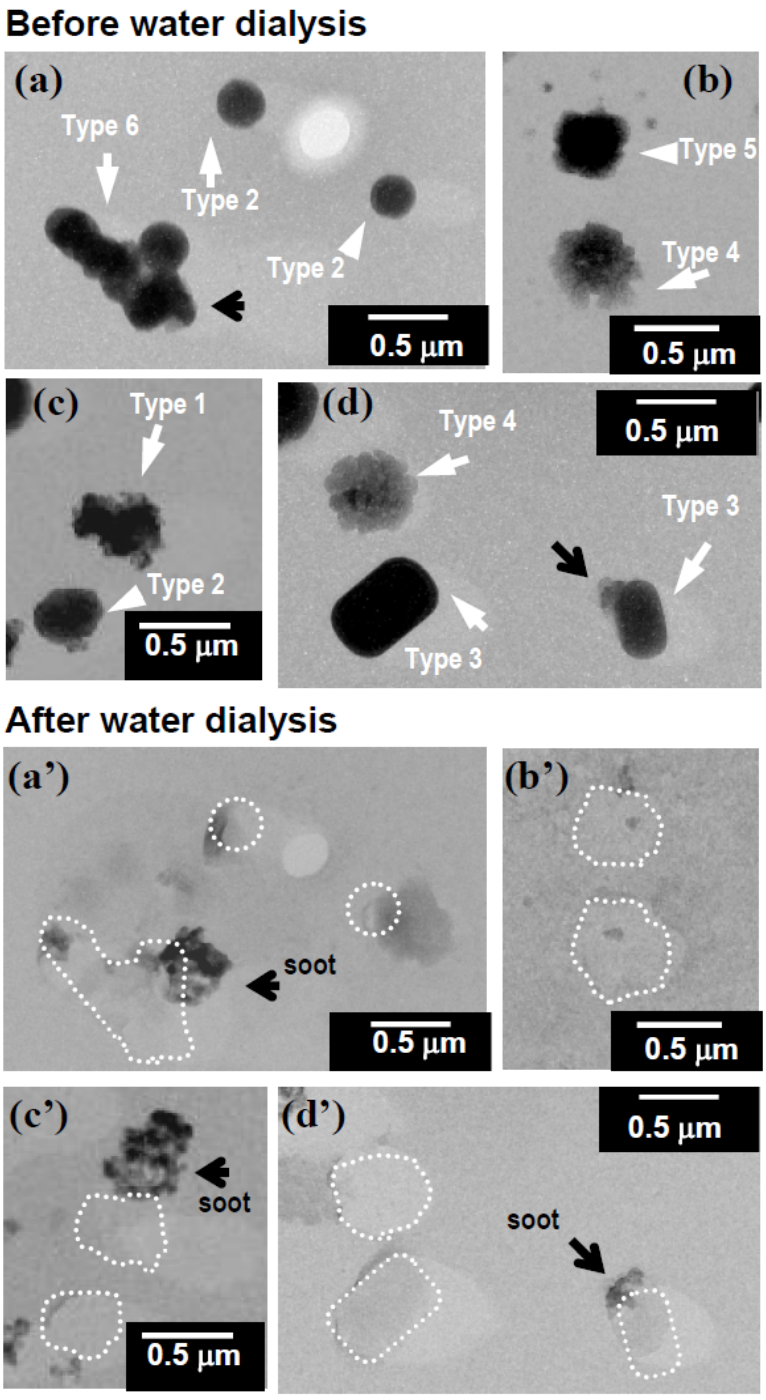

Figure 3-8 Electron micrographs before and after water dialysis for Type 1–6 particles. (a), (b), (c) and (d): before water dialysis. (a'), (b'), (c') and (d'): after dialysis with water for the same regions of (a), (b), (c) and (d) respectively. White arrows indicate morphological types. White dotted lines represent peripheral positions of particles before water dialysis. Black arrows indicate insoluble-soot cores.

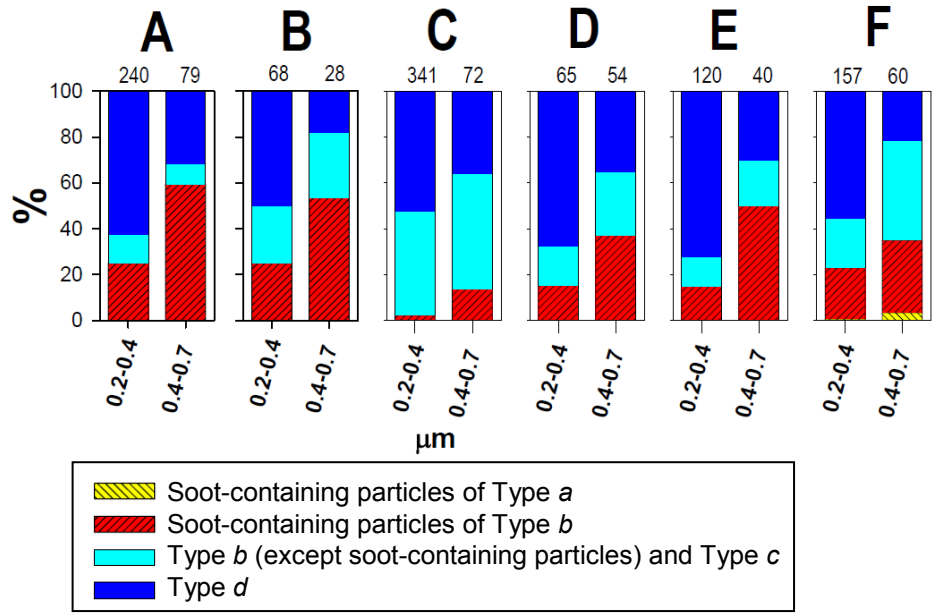

Figure 3-9 Number proportions of mixing states between soluble/insoluble materials for particles in samples A–F. Classification of mixing states are as shown in Figs. 2-4 and 2-5. Numbers shown above columns represent the numbers of particles observed.

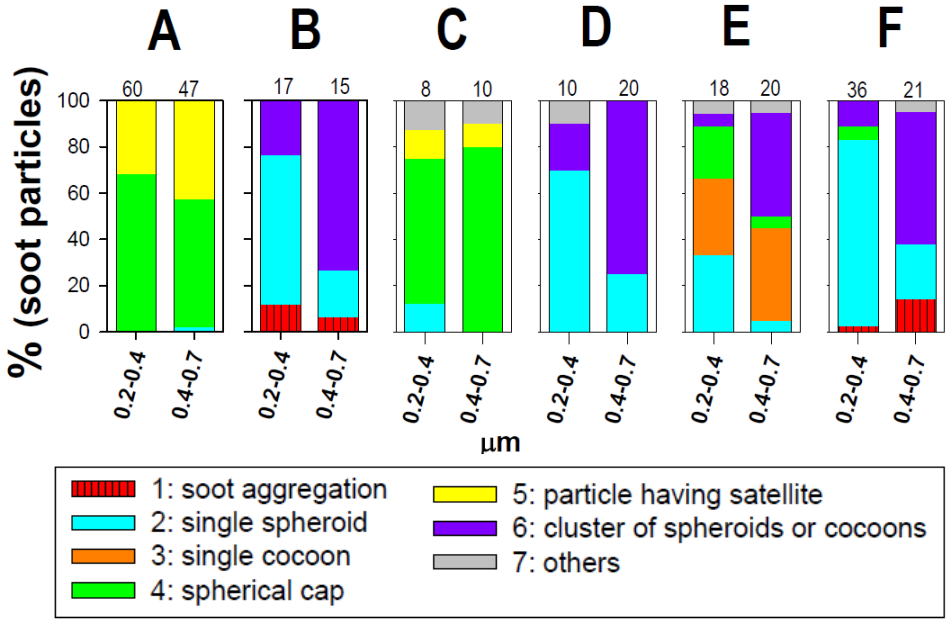

Figure 3-10 Number proportions of morphological types before water dialysis of soot-containing particles for samples A–F. Classification of morphological types 1–6 were the same as Fig. 3-5. Numbers shown above columns represent the numbers of soot-containing particles observed.

and were found in only sample F. Most soot-containing particles on samples A–F were mixed with water soluble materials (i.e. Type *b*). The number proportions of soot-containing particles of 0.4–0.7 μm were higher than those in the 0.2–0.4 μm for all samples. Number proportions of the soot-containing particles ranged from 2% (sample C) to 25% (samples A and B) for 0.2–0.4 μm and 14% (sample C) to 59% (sample A) for 0.4–0.7 μm. These almost identical the same ranges to those found in moderately remote atmospheric samples [*Pósfai et al*., 1999; *Hasegawa and Ohta*, 2002]. In contrast, the number proportions of Type *d* (water-soluble particles without insoluble materials) were high (>50%) in 0.2–0.4 μm but low (<36%) in 0.4–0.7 μm in diameter.

For only soot-containing particles, Fig. 3-10 presents number proportions of morphological types before water dialysis. Number proportions for soot-containing particles in Fig. 3-10 showed a similar tendency to that depicted in Fig. 3-6 for each sample: high proportions of Types 4 and 5 irrespective of size range in samples A and C, and high proportions of Type 2 or 3 for 0.2–0.4 μm and Type 4 or 6 for 0.4–0.7 μm in samples B, D, E, and F

3.6. Volume fraction of soluble materials of soot-containing particles

The mixing state of soot with water-soluble materials is expressed quantitatively as volume fraction (ε) of water-soluble material in individual particles. Combined with water dialysis and shadowing methods [*Okada*, 1983], ε is estimated as follows,

$$\varepsilon = \left(1 - \frac{Vol_{after\_dialysis}}{Vol_{befre\_dialysis}}\right) \times 100 \ [\%] \qquad (3\text{-}1)$$

where $Vol_{after\_dialysis}$ and $Vol_{beforer\_dialysis}$ is volume of a particle respectively before and after water dialysis.

Figure 3-11 shows box plots of ε (a and c) and diameter of insoluble core (b and d) for soot-containing particles (a and b for 0.2–0.4 μm, c and d for 0.4–0.7 μm) in samples A–F. Size range were separated at 0.4μm similar to that in Fig. 3-10 because dominant morphological feature differed with size: abundant for single ball (Type 2) and single cocoon (Type 3) particles in 0.2–0.4 μm and clustered particles (Type 6) in 0.4–0.7 μm for samples B, D, E, and F. The median values of the ε for 0.2–0.4 μm and 0.4–0.7 μm were respectively higher than 80% and 90% (Figs. 3-11a and 3-11c), indicating that most of soot-containing particles comprised large amounts of soluble materials. The median values of insoluble core diameters in soot-containing particles were, respectively, 0.1–0.2μm and 0.1–0.25 μm for particle size ranges of 0.2–0.4 μm and 0.4–0.7 μm (Figs. 3-11b and 3-11d). Insoluble core diameters were almost identical, irrespective of the size range. Therefore, larger values of ε for 0.4–0.7 μm imply further addition of soluble materials with growth of their size.

The ε values for soot-containing particles at Cape Hedo were almost identical to the average values (8–28%) of soot volume fractions for particles 0.15–0.8 μm at an urban background site in Mainz, Germany [*Vester et al.*, 2007] and median value (15%) of soot volume fractions for particles 0.05–0.3μm at Mexico City [*Adachi and Buseck*, 2008]. The time evolution of the aerosol size distribution over the Mexico City plateau was simulated well with heterogeneous condensation of semi-volatile materials onto initial aerosol particles [*Kleinman et al.,* 2009]. Although such analyses during transport from the source region cannot be provide in this study, the source strength and resultant possibility will be addressed as follows. Based on observation using Q-AMS at a rural site in southern China, *Xiao et al.* [2009] examined the rapid growth of aerosol particles

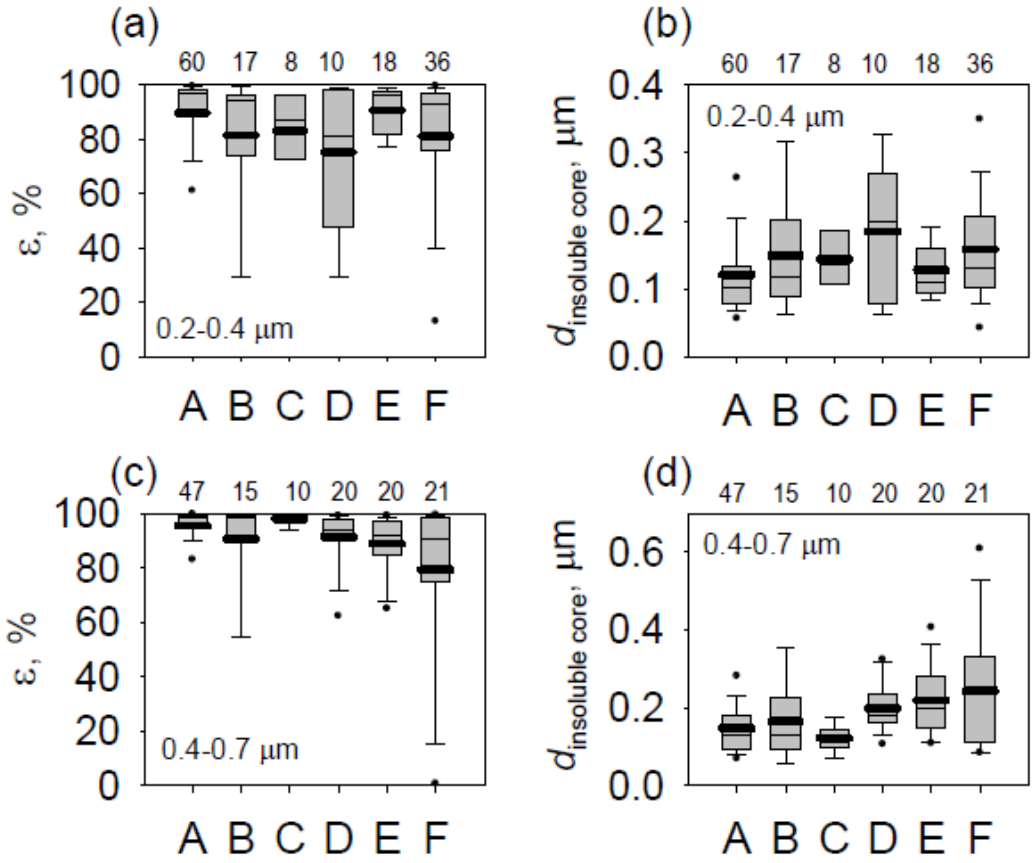

Figure 3-11 Box plot of volume fraction (ε) of soluble materials (a and c) and diameter of insoluble materials (b and d) in individual soot-containing particles of 0.2–0.4 μm and 0.4–0.7 μm for samples A–F. The lower boundary of the box indicates the 25th percentile, the line within the box marks the median, and the upper boundary of the box indicates the 75th percentile. Whisker above and below the box indicate 90th and 10th percentiles. The mean is also drawn as a thick line. Numbers shown above boxes represent the numbers of soot-containing particles observed.

from ca. 140–170 nm within 3 hr. They found that heterogeneous condensation of oxygenated organic carbons and H_2SO_4 oxidized from SO_2 of ca. 3–21 ppbv explained that rapid growth. Increased particle diameter from 140 to 170 nm and 193 nm respectively represent about 50% and 90% increase in particle volume. According to surface air measurements using passive samplers [*Meng et al.,* 2010], the annual average SO_2 concentrations in 2008 were 9 and 15 ppbv, respectively, for Huaian and Lin'an, which are both located near the coast of eastern central China, along the backward air trajectories computed for the samples in this study. The SO_2 concentrations in eastern central China were comparable to those reported by *Xiao et al.* [2009]. Therefore, accumulation mode particles from the coast of eastern central China might have grown by 90% by volume after condensation of H_2SO_4 and oxygenation of organic carbons before arriving at Cape Hedo.

For soot-containing particles of 0.2–0.4 μm in samples A, C and E, values of ε were somewhat higher than those in samples B, D, and F collected under high aerosol number concentrations. Assuming the same SO_2 concentrations at eastern central China, because higher (lower) aerosol number concentration supplies larger (smaller) condensation sink proportional to their total surface area, amount condensed on a particle under high (low) aerosol concentration might be smaller (larger) than that in low (high) aerosol concentration. Although large variations with lower ε on samples B, D and F is not explained enough by this simple partitioning, slightly higher median and average values of the ε in samples A, C, E might be able to attribute to lower condensation sink during transport.

3.7. Formation of clustered particles

Cluster-like particles were dominant (>60%) in larger size range (>0.4 μm) for samples B, D, and F depicted in Fig. 3-6. In the larger size range of samples B, D, and F, 32–54% of particles were soot-containing particles (Fig. 3-9) and 57–75% of soot-containing particles were clustered particles. Although similar clustered particles have been reported, but connected with tar-balls [*Hand et al.*, 2005] or balls of electron-beam-sensitive materials [*Vester et al.,* 2007], the formation process of clustered particles have not been discussed in detail.

Soot particles in the atmosphere are subjected to several aging processes such as condensation of semi-volatile gaseous species [*Zhang and Zhang*, 2005; *Pagels et al.*, 2009; *Khalizov et al.*, 2009a, 2009b], coagulation with other aerosols [*Jacobson*, 2001], and cloud processing [*Huang and Yu*, 2008]. Among these processes, because (1) condensation cannot connect particles of similar size as a cluster and (2) swelling by cloud processes does not form clustered particles to minimize the surface-to-volume ratio, only coagulation processes with collision and adhesion of solid particles can form clustered particles. Morphological differences among samples might provide clues to understanding the formation process of clustered particles.

As depicted in Fig. 3-6, two patterns were found in remarkable morphological types of particles with satellite structure (samples A and C) and cluster shape (samples B, D, E and F). According to Q-AMS results (Table 3-1), molar ratios of NH_4^+/SO_4^{2-} for samples A and C were close to unity, suggesting ammonium bisulfate as the major constituent. The deliquescence humidity of ammonium bisulfate is 39% RH [*Tang*, 1977]. The relative humidity of outside air during the sampling period of A and C was higher than this value (71% and 53%, respectively). Therefore, most aerosol particles had been deliquesced and transformed into spherical droplets to minimize the surface area to the

volume ratio in the atmosphere. Indeed, particles showing a satellite structure were abundant but clustered particles were not found in sample A or C. For samples B, D, E, and F, the results of Q-AMS suggested the existence of ammonium sulfate. Based on meteorological conditions along the trajectory computed using HYSPLIT 4, maximum (average) values of relative humidity along the trajectory from the coast of China for samples B, D, E, and F were, respectively, 78(66), 76(53), 74(55), and 86 (52)%. The maximum relative humidity for samples B, D and E were lower than the deliquescence humidity (80% RH) of ammonium sulfate [*Tang et al.*, 1981]. Therefore, most aerosol particles for samples B, D and E were solid in the atmosphere consistent with coagulation formation of clustered particles. However, high relative humidity for samples F is enigmatic because of the possibility of deliquescence during transport. For sample F, organics constituted 27% of total mass measured by Q-AMS. *Saxena et al.* [1995] reported that mixing with organics (possibly film forming hydrophobic substances) might reduce water absorption of inorganic aerosols in urban condition. Although maximum relative humidity during transport for sample F was slightly higher than deliquescence humidity of ammonium sulfate, the relative humidity, on average, was 52%. Considering the uncertainty of HYSPLIT output and potential mixture with large amount of organics, aerosol particles for sample F could not be deliquesced during transport. As inferred from morphological differences among samples, cluster-shape particles might be formed by coagulation processes of spheroidal solid particles under dry conditions. Further discussion about formation processes of cluster-shape particles will be showed using a simple coagulation model during transport time from the source area.

Aerosol particles collide and stick together because of coagulation under high aerosol concentration condition. Therefore, the average aerosol particle size increases

concomitantly with decreasing number concentration over time. The rate of coagulation is proportional to the number concentration and the coagulation coefficient, K, depending mainly on the particle size and diffusion coefficient. Assuming that particles adhere at every collision, then the general coagulation equation can be written as

$$\frac{dN_k}{dt} = \frac{1}{2}\sum_{j=1}^{k-1} K_{j,k-j} N_j N_{k-j} - N_k \sum_{j=1}^{\infty} K_{k,j} N_j \qquad k \geq 2\,, \qquad (3\text{-}2)$$

where N_k represents the number concentrations of k-mer particles formed by collision of a (k-j)-mer with a j-mer of a single unit particle [*Seinfeld and Pandis*, 2006]. In this formulation, it is assumed that the smallest particle is of size k=2, a dimer. The coagulation coefficient ($K_{p,q}$) between a p-mer and a q-mer particle is calculated from equation (3).

$$K_{p,q} = 2\pi\left(d_p + d_q\right)\left(D_p + D_q\right) \qquad (3\text{-}3).$$

Therein, d_p and d_q respectively denote diameters of particles for p-mer and q-mer of unit particle. Also, D_p and D_q respectively represent Brownian diffusion coefficients for particles for p-mer and q-mer, assuming standard atmospheric conditions (293K and 1013 hPa). The volume equivalent diameter was used as the particle diameter after collision. Particles after coagulation are able to form various shape and length. The value of coagulation coefficient using volume equivalent diameter is lower than that for actual shape. Using these equations, number concentrations of total (k-mer plus j-mer with monomer) particles and k≥2 particles as coagulated particles (collided more than once) were estimated to distinguish non-coagulated particles. Although the monodisperse situation is assumed for initial condition, the estimates are sufficiently accurate to be

useful as approximations for atmospheric aerosols and to provide insight into the importance of coagulation in this situation.

In this estimation, it must assume (1) the initial diameter of particles ($d_{k=1}$), (2) the initial number concentration of aerosols ($N_{k=1,\ t=0}$), and (3) the time of coagulation. The initial diameters of particles are approximated as 0.3 μm because of the size of a single unit in clustered particles. Number concentrations of aerosols are assumed from observation values at Beijing [*Wu et al.,* 2008] and Cape Hedo in this study. According to *Wu et al.* [2008], number concentrations of aerosols (>0.1 μm) in the urban atmosphere of Beijing were 7100, 11,200, 38,400 cm^{-3}, respectively, for the annual median, 75% percentile and maximum values. At Cape Hedo, number concentrations of 0.2–0.5 μm particles were 300–900 cm^{-3} for the period of samples B, D, E and F (Table 3-1). Consequently, initial number concentrations were set to 1) 500 cm^{-3} to represent number concentrations at Cape Hedo, 2) 2000 cm^{-3} as a geometric mean value between 1) and 3), and 3) 7000 cm^{-3} as the aerosol concentration at Beijing. In reality, dilution by clean air during transport to Cape Hedo can also reduce number concentration at windward area, in addition to reduce by coagulation. Therefore, using number concentration at Cape Hedo as an initial value intends to show the least value. Based on backward air trajectory analysis, transportation times from source areas were 1–5 days for the samples in this study. Consequently, the duration of the coagulation estimate is set for 5 days.

Figure 3-12 presents the estimated number concentrations of total particles (N_{total}) and the number proportion of coagulated ($k \geq 2$) particles to the total number concentration as a function of time. The number concentrations for initial conditions of 500 cm^{-3}, 2000 cm^{-3} and 7000 cm^{-3}, respectively decreased to ca. 480 cm^{-3}, 1700 cm^{-3}

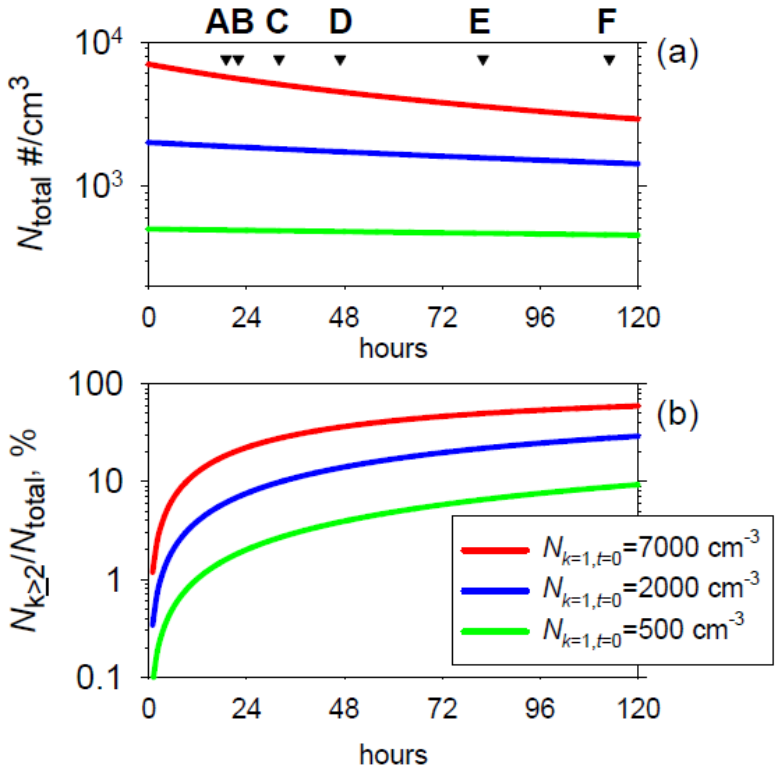

Figure 3-12 (a) Number concentration of particles (N_{total}) and (b) number fraction of coagulated particles ($N_{k\geq2}$) to total particles as a function of time. For samples A–F, transport hours from the coast of China are shown as inverted triangles in the upper panel.

and 4500 cm^{-3} during first two days by coagulation process (Fig. 3-12a). The 480 cm^{-3} is almost comparable with the observed number concentrations (440 cm^{-3} for 0.2–0.5 μm) at Hedo for sample D with transport time of two days. The number proportion of coagulated particles to total particles increased more rapidly at higher (7000 cm^{-3}) initial number concentrations in Fig. 3-12a. The number proportions of coagulated particles to total particles respectively increased 4%, 14%, and 37% after two days for 500 cm^{-3}, 2000 cm^{-3} and 7000 cm^{-3} of initial concentrations (Fig. 3-12b). In other words, the number concentrations of coagulated particles after two days were respectively, 20 cm^{-3}, 240 cm^{-3} and 1600 cm^{-3}. The observed number concentration of 0.3–0.5 μm for sample D was ca. 100 cm^{-3}. Considering that the number proportion of clustered particles in sample D were 72% for 0.4–0.7 μm particles, the number concentration of clustered particles in the atmosphere was presumably less than 72 cm^{-3}. This number concentration of clustered particles is higher than estimated value (20 cm^{-3}) using the initial concentration at Hedo, but lower than values (1600 cm^{-3}) using data in Beijing. Based on back calculation, coagulated particles of 70 cm^{-3} after two days can be estimated by assuming initial number concentration of 1000 cm^{-3}. These results indicate that the number concentration of observed clustered particles can be explained by coagulation process under the condition of number concentrations between Cape Hedo and Beijing. Therefore the estimated values for transport time of two days reasonably agree with observed number proportion of clustered particles in sample D.

3.8. Implications of soot-containing cluster particles

The size distribution of light absorption coefficient portrayed in Fig. 3-4 was a bimodal distribution with modal diameters at 0.3–0.4 μm and 0.5–0.6 μm. Particles of

larger modes mainly comprised clustered particles. As discussed in section 3.7, clustered particles of the larger mode were presumably formed by coagulation processes. Although such larger mode particles had been often attributed to origination from cloud processing or volume condensation [e.g., *Meng and Seinfeld*, 1994; *Huang and Yu*, 2008], particles of coagulation clusters formed under dry conditions might also be important for aerosol size evolution in the atmosphere. It is noteworthy that sufficiently high aerosol concentrations with abundant soot are expected for leeward areas of megacities during several days of outflow. According to *Adachi et al.*, [2010], the values of absorption and direct forcing estimated from a core-shell model were overestimated by ca. 30% and ca. 20%, respectively, compared to those estimated for irregular shaped soot-containing particles internally mixed with organic matter in Mexico City. As this study discussed, coagulation processes alter the number concentration and proportion of irregularly (non-spherical) shaped particles under conditions of dry and high aerosol concentration. Direct radiative effects of aerosols in the atmosphere occur under clear skies, under possibly dry conditions, which is important for considering formation of larger irregularly shaped soot-containing particles by coagulation at the leeward areas of megacities.

3.9. Chapter summary

Atmospheric aerosol particles in continental outflow from eastern Asia were observed at Cape Hedo, Okinawa in Japan. Six samples of aerosol particles derived from eastern central China during 1–5 days were analyzed for morphological features and mixing states of soot-containing particles (0.2–0.7 μm) using water dialysis under TEM observation. Number proportions of the soot-containing particles ranged from 2%

(sample C) to 25% (samples A and B) for 0.2–0.4 μm and 14% (sample C) to 59% (sample A) for 0.4–0.7 μm. Most soot-containing particles were mixed internally with large volume of soluble materials: the median values of the ε (soluble to total volume in %) for 0.2–0.4 μm and 0.4–0.7 μm were respectively higher than 80% and 90%. The median values of insoluble core diameters in soot-containing particles were, respectively, 0.1–0.2 μm and 0.1–0.25 μm for particle size of 0.2–0.4 μm and 0.4–0.7 μm. Results of EDX elemental analyses of individual particles and Q-AMS aerosol chemical measurements at the site suggest that soluble materials in samples mainly consist of NH_4^+, SO_4^{2-}, and organics.

For samples consisted mainly of ammonium sulfate and organics, soot-containing particles were spheroidal or cocoon-shaped for 0.2–0.4 μm. Particles showed a clustered shape, with connected multiple units (about 0.3 μm in diameter), for larger sizes. The shapes and sizes of single units of clustered particles resembled those of spheroidal particles or cocoon-shaped particles in the same sample, implying the formation of clustered particles through coagulation processes. Morphological information related to soot-containing particles is used to improve our understanding of soot aging process. The number proportions of coagulated particles to total particles were estimated using a simple coagulation model with appropriate initial conditions adapted to our observations. Estimated number concentration of particles coagulated for two days reasonably agree with observed number proportion of clustered particles, which suggests that coagulation clusters might also be important for aerosol size evolution in polluted atmosphere. Formation of larger soot-containing cluster particles by coagulation must be considered for climatic assessment for aerosol effect from megacities.

4. Change of population and mixing states of cloud interstitial soot particles at Mt. Tateyama, Japan

In-cloud scavenging process is an important process to evaluate of spatial distribution and long-range transport of soot-containing particles in the atmosphere. Although in-cloud scavenging process is a dominant process to remove submicron aerosol particles as explained in section 1-3, some aerosol particles were left behind after in-cloud scavenging process. Cloud-forming potential of an aerosol particle depends on size and mixing states of the particles with soluble materials. Because aerosol particles left behind in cloud interstitial air have less chance to be collected by rain drops, particles having less cloud-forming potential such as less-aged soot particle might have some higher likelihoods of surviving longer in the atmosphere. Change of population and mixing states of soot-containing particles in cloud interstitial air is important to consider amount and optical property of soot-containing particles after in-cloud scavenging process. This chapter focuses on modification of mixing states of hydrophobic and hygroscopic soot-containing particles, and presents mixing states of cloud interstitial aerosol particles collected at a Mountain site and discussions about controlling factors of the mixing states.

4.1. Atmospheric observation at Mt. Tateyama

To investigate cloud interstitial aerosol particles under fog conditions, atmospheric observations were conducted at Tengudaira (36°24'N, 137°34'E, 2300 m a.s.l.) of Mt. Tateyama, Japan during June 20−25 in 2007. Figure 4-1 portrays a location map of the observation site at Mt. Tateyama. The site is located at about the forest limit in a natural preserve, where it is isolated from industrial urban areas. Details about Mt. Tateyama

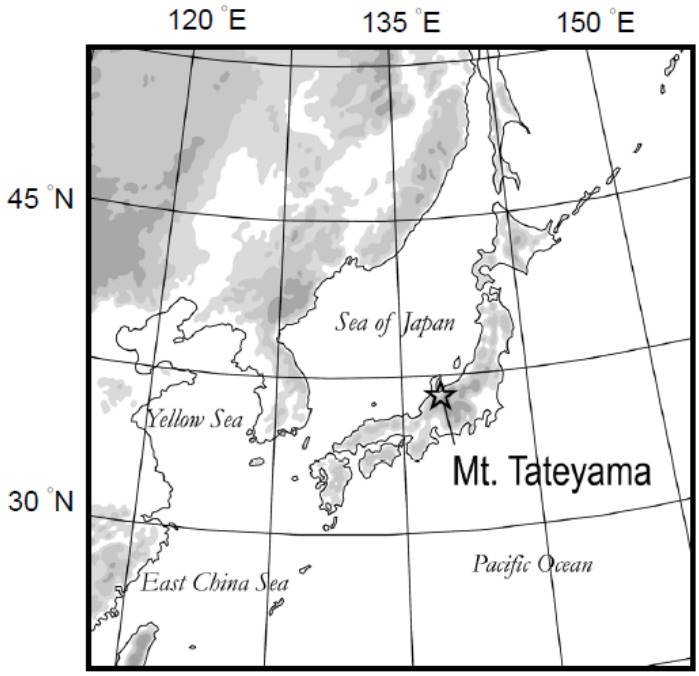

Figure 4-1 Location of Mount Tateyama, Japan.

and daily and seasonal variations of aerosols at Murododaira (36°57'N, 137°60'E, 2450 m a.s.l.) were reported by *Osada et al.* [2003]. We set our measurement systems on the second floor of a mountain lodge at Tengudaira. The inlets were placed at about 5 m above the ground. To separate fog droplets and interstitial particles, impactors having aerodynamic 50% cut off diameter of 10 μm were used for sampling lines. Weather conditions such as the visual density of fog were monitored periodically (5 min interval) at the site using a digital camera. Air temperature and relative humidity were recorded every 10 min using a portable data logger (MR6600; Chino Corp.). Hourly precipitation data were obtained from a meteorological observatory at Kamiichi (296 m a.s.l.) located 15 km northwest of Tengudaira.

4.2. Temporal variation of meteorological conditions and aerosol parameters

Figure 4-2 portrays temporal variations in meteorological elements and aerosol properties during observations of 20–25 June 2007. Figure 4-2a shows temperature and relative humidity at the observation site and hourly precipitation at Kamiichi. Figure 4-2b presents weather conditions (fog and rain) at this site. During fog events of 21−22 and 24−25 June, the relative humidity was nearly 100%. Figure 4-2c presents the number concentrations N_T (01−0.3 μm and 0.3−0.5 μm in diameter) and volume concentrations V_p (0.1−0.5 μm diameter) of aerosol particles measured using the LPC system presented in Fig. 2-4. The volume concentrations were calculated from number concentrations for each size range of the LPC and their geometric mean diameters assuming spherical particles. Number concentrations of aerosols decreased about one to two orders of magnitude during rain or fog, as shown for June 21–22 and 24–25 in Fig. 4-2c. Average number concentrations of 0.1–0.3 μm and 0.3–0.5 μm diameter particles

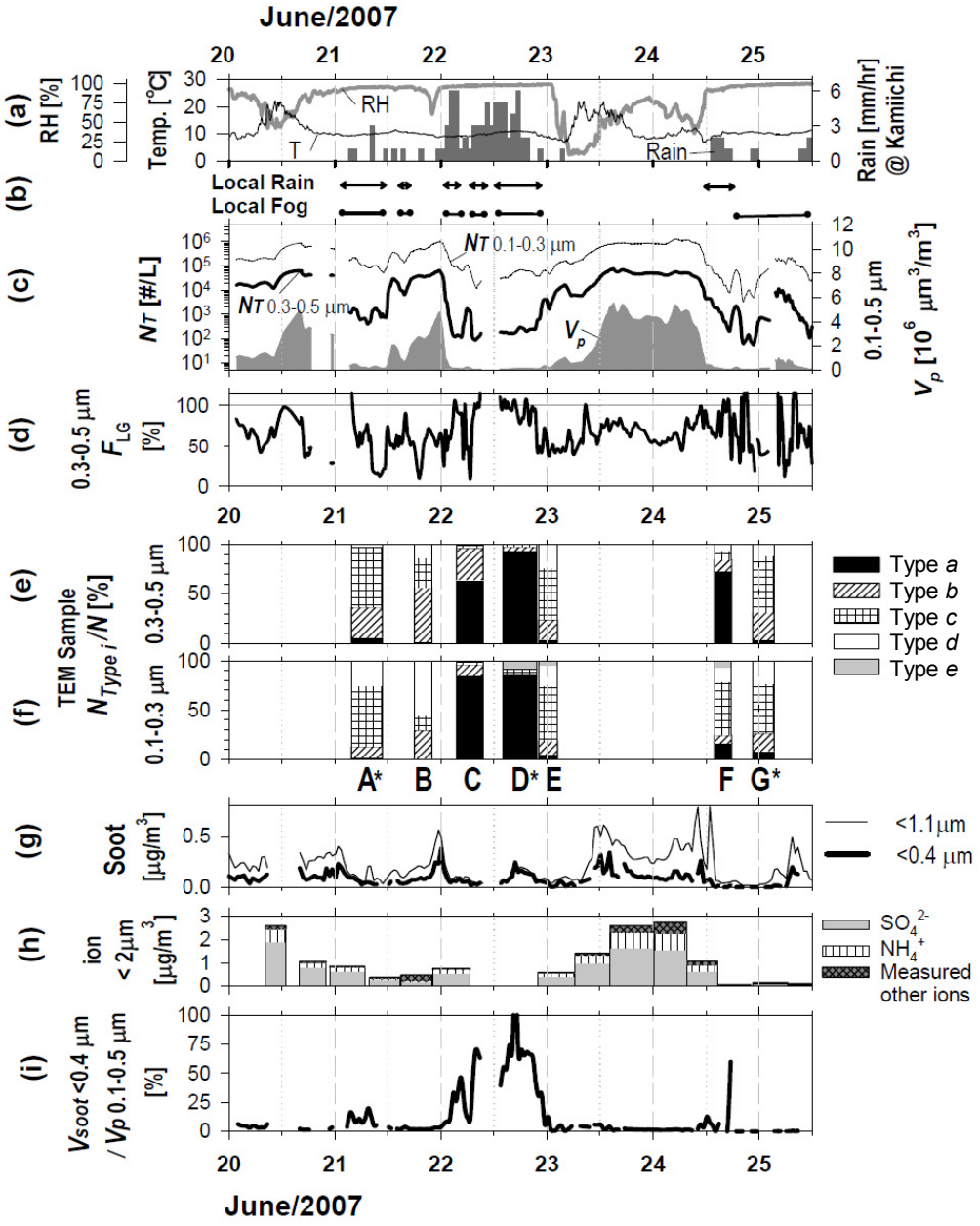

Figure 4-2 Temporal variations of (a) temperature (thin black line) and relative humidity (thick gray line) at this site and precipitation at Kamiichi (dark gray bars), (b) duration of rain and fog, (c) number (thin and thick black lines) and volume (area plot) concentrations of aerosols with 0.1−0.5 μm diameter, (d) number fraction of LG particles with 0.3−0.5 μm in diameter, (e, f) number proportions of the five types of LG particles with 0.3−0.5 and 0.1−0.3 μm diameter by TEM, respectively, (samples with asterisks are cloud interstitial samples), (g) soot mass concentration, (h) ionic mass concentration, and (i) ratio in % of soot volume ($V_{\text{soot}\ <0.4}$) per particle volume ($V_{\text{p}\ 0.1-0.5}$).

Table 4-1 TEM samples with meteorological conditions. Relative humidity is listed as first and second hygrometer data in the sampling flow diagram.

Sample	Sampling period (LST)		Time	Relative Humidity [%]		Weather	Number of analyzed particles
ID	start	stop	[min]	1st	2nd		
A	2007/6/21 3:46	6/21 10:44	418	89–91	35–37	Fog and Rain	859
B	2007/6/21 17:59	6/21 21:59	240	84–88	34–43	Cloudy	962
C	2007/6/22 3:33	6/22 9:33	360	88–89	41–44	Partly Fog and Rain	389
D	2007/6/22 14:05	6/22 21:40	455	84–87	32–23	Fog and Rain	326
E	2007/6/22 22:08	6/23 2:23	255	87–88	21–38	Fog, later Fair	630
F	2007/6/24 13:56	6/24 17:46	230	88–90	32–41	Rain	457
G	2007/6/24 22:35	6/25 3:24	289	85–88	40	Fog	673

during the entire observation period were 3.4×10^5 L^{-1} and 1.9×10^4 L^{-1}. They were, respectively, 6.2×10^5 L^{-1} and 3.7×10^4 L^{-1} after excluding data obtained under rain and fog conditions. Figure 4-2d presents F_{LG} with diameters of 0.3–0.5 μm. The F_{LG} varied from about 10% to 100%, with the average of 67% during this period. Number proportions of morphological types of LG particles based on water dialysis are presented in Fig. 4-2e (0.3−0.5 μm diameter) and 6f (0.1−0.3 μm diameter). Details of the TEM samples and the number of analyzed particles are presented in Table 4-1. As indicated for samples D and F in Fig. 4-2e, water-insoluble particles (Type *a*) were dominant during high F_{LG} (nearly 100%). For samples A, B, E, and G with moderate (around 50%) F_{LG}, most particles in the samples were classified as Types *b* and *c*, comprising partly water-soluble materials in a particle. These results suggest that values of F_{LG} correspond to the number ratio of water-insoluble to total particles for a given size range (0.3−0.5 μm diameter). Comparison of particle types in Fig. 4-2e with those in Fig. 4-2f reveals that the proportions of water-soluble particles (Type *d*) of 0.1–0.3 μm diameter in samples A, B, F, and G were higher than those of 0.3–0.5 μm diameter. Some water-soluble particles in the 0.1–0.3 μm diameter range might not grow sufficiently large to be removed by the impactor of our sampling system. For samples C and D, water-insoluble particles (Type *a*) were dominant for both 0.1–0.3 μm and 0.3–0.5 μm diameter.

Figures 4-2g and 4-2h respectively portray soot and ionic mass concentrations in aerosols. During our observations, soot (<1.1 μm diameter) and ionic (<2 μm diameter) mass concentrations were, respectively, about 0.0–0.8 μg m^{-3} and 0−3 μg m^{-3}. Size ratios (<0.4 / <1.1 μm diameter) of soot mass concentrations were about 0.5 during the observation. However, on 22 June, soot particles were mostly smaller than 0.4 μm diameter. Major ionic species were NH_4^+ and SO_4^{2-}. The volume concentration of soot

(V_{soot}) was estimated by assuming the soot density as 1.8 g cm^{-3}. Figure 4-2i portrays ratios of V_{soot}(<0.4 μm diameter) to volume concentration of particles V_p (0.1–0.5 μm diameter). The volume fractions of soot were usually less than 10%, but increased to nearly 80% during high F_{LG} when high proportions of Type *a* particles were found on 22 June. As described above, F_{LG} is related to the degree of external mixing of water-insoluble and soluble particles. The F_{LG} value is obtainable both continuously and easily. Therefore, it will be useful to provide meaningful and representative aerosol sampling for labor-intensive TEM analyses.

4.3. Features of interstitial particles under fog conditions

The TEM samples of A on 21 June, D on 22 June, and G on 24–25 June were collected under fog conditions with stable F_{LG} and aerosol number concentrations. The F_{LG} values for samples A and G were approximately 50%, although the F_{LG} for sample D was very high: nearly 100% (Fig. 4-2d). This section presents discussion of the morphological features of cloud interstitial and LG particles during fog events based on TEM analyses.

Figures 4-3 respectively present TEM images of samples A and G before (a) and after (b) water dialysis. Images of (b) show the same sample region at the same magnification as (a). Dominant particles in samples A and G were Type *c* (61% and 57%, respectively) having residual materials after water dialysis (e.g. arrowed particles in Figs. 4-3). Figure 4-3c presents examples of morphological changes of particles before and after water dialysis, and after strong irradiation of electron beams. After irradiation by strong electron beams, most semi-transparent residual materials in samples A and G were evaporated, as shown by particles in Figs. 4-3c. Sulfate and some organics are

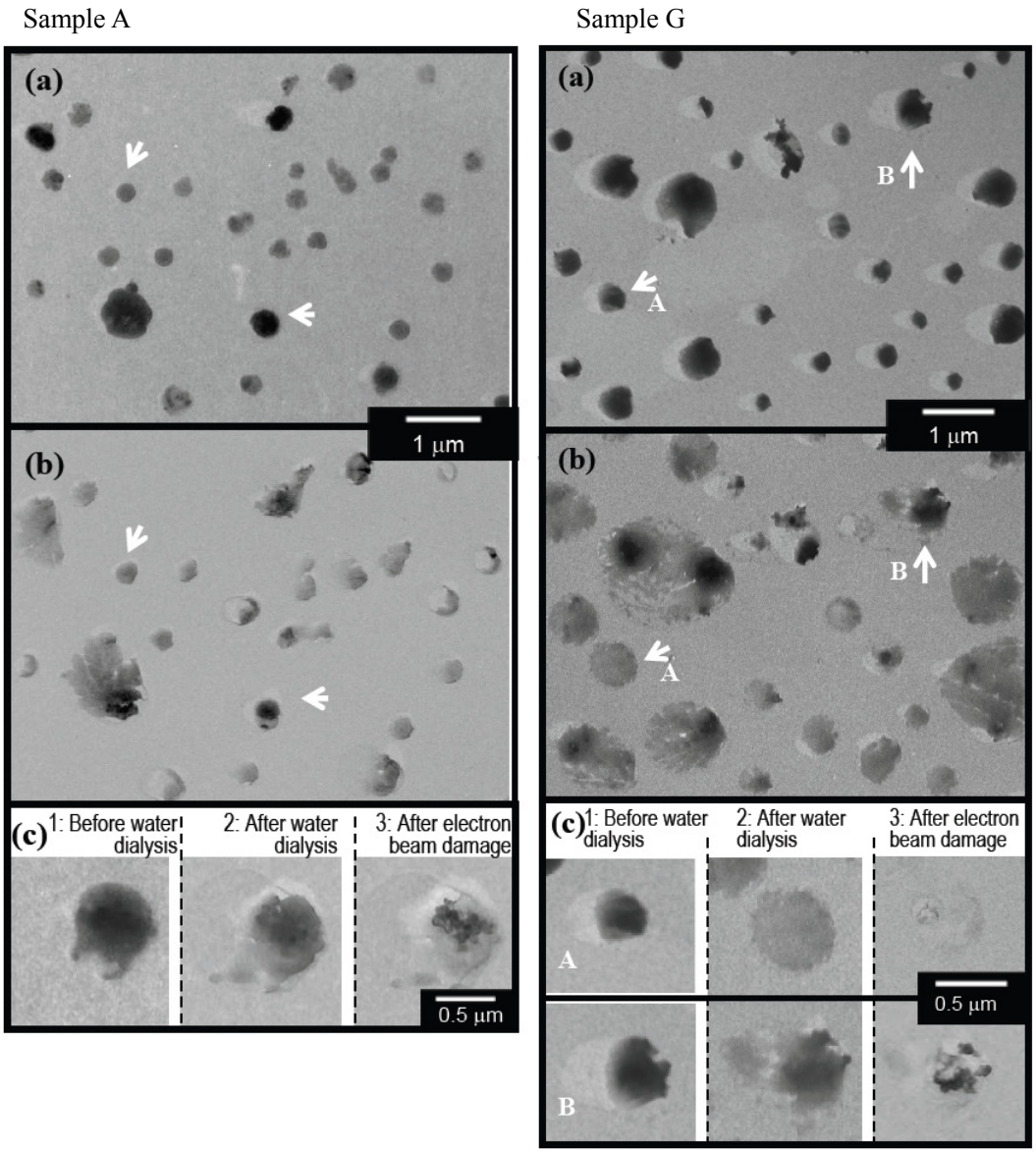

Figure 4-3 Electron micrograph of cloud interstitial sample A and G at Mt. Tateyama: (a) before and (b) after dialysis with water for the same sample region. Arrow-indicated particles A, B, C and D are partially soluble particles after water dialysis. (c) morphological changes of a particle. 1, before water dialysis (left). 2, after water dialysis (middle). 3, after strong irradiation of electron beams (right).

electron-beam-sensitive materials [*Pósfai et al.,* 1999; *Buseck and Pósfai*, 1999]. In about 20% of Type *c* particles (e.g., particles of Fig. 4-3c) in samples A and G, insoluble agglomerate inclusions were found after irradiation. In addition to morphological TEM analysis, we examined elemental compositions of residual materials using SEM-EDX. In fact, Si and Al were not detected. Therefore, residual materials of samples A and G are not mineral dusts. Elements found after subtracting the carbon-covered collodion film (background) were C (>50%), O, and rarely S in the order of occurrence, suggesting that the residual materials might be organics with a somewhat beam-resistant nature.

The average F_{LG} during the collection of sample D was 92%. Based on the dialysis of sample D, 93% of LG particles with 0.3–0.5 μm diameter were Type *a* (water-insoluble). Figure 4-4 presents TEM images of sample D before (a) and after (b) water dialysis and magnified images of some residual materials after water dialysis (c and d). As shown by arrows in Figs. 4-4a and 4-4b, and Fig. 4-4c, particles comprising chain aggregations of water-insoluble spherules were often observed. Such chain aggregations were often regarded as soot particles [*Janzen*, 1980; *Pósfai et al.*, 2004; *Murr and Soto*, 2005]. These aggregated particles constituted 54% of water-insoluble particles after dialysis in sample D. As already presented in Fig. 4-2i, the volume ratio of soot (<0.4 μm diameter) to total aerosol (0.1–0.5 μm diameter) on 22 June was high (70%) with a high F_{LG} (92%). Combined with high soot fractions in aerosols under fog conditions with the result obtained using water dialysis, cloud interstitial particles during sample D are suggested to be mainly soot particles with few soluble materials.

In our study, the soot mass concentration during the collection of sample D was mostly found in the size range of particles smaller than 0.4 μm (Fig. 4-2g), although the ratio of <0.4/<1.1 μm for soot was about 0.5 for the remainder of the period. The size distribution of soot might be changed by aging processes after emissions. In fact, *Huang*

Sample D

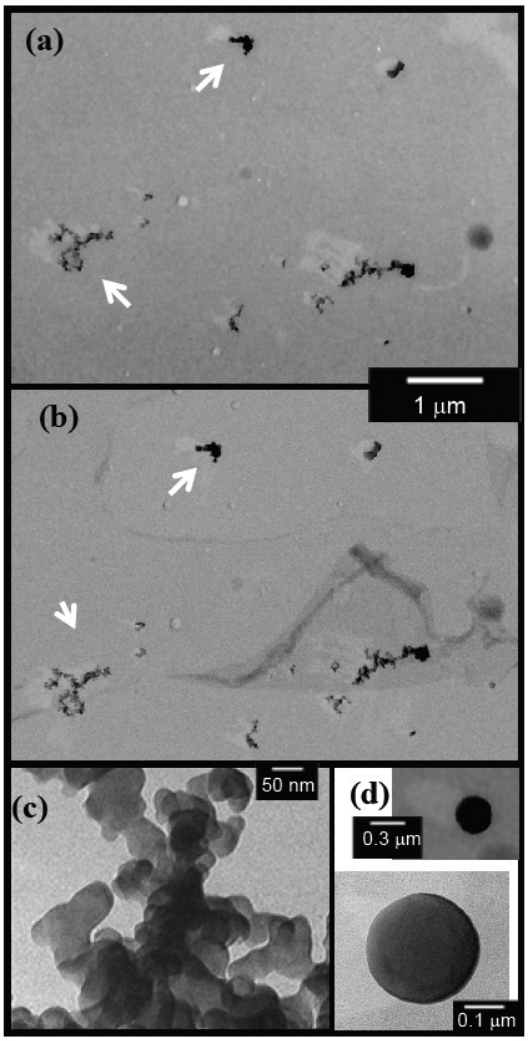

Figure 4-4 Electron micrograph of cloud interstitial particles in sample D: (a) before and (b) after dialysis with water for the same sample region. Arrow-indicated particles E and F are chain-like soot particles without water-soluble materials. (c) magnified image of chain-like particle after dialysis. (d) magnified images of spherical "tar ball" after dialysis.

et al. [2006] and *Huang and Yu* [2008] reported the size distribution of freshly emitted elemental carbon (EC) in a roadway tunnel in southern China and compared it with that in the urban atmosphere. The mode diameter of freshly emitted EC in the tunnel (0.32−0.56 μm diameter) was smaller than that in the urban atmosphere (0.32−1.0 μm diameter). They reported that the larger mode diameter of soot particles was attributed to growth after aging processes in the urban atmosphere. For sample D, considering that larger (> 0.4 μm) soot-containing particles were probably mixed with soluble materials after aging processes, they might act efficiently as CCN and scavenged to cloud droplets. Consequently, smaller (< 0.4 μm) soot particles without soluble materials might become dominant in the cloud interstitial air of sample D. Because fog and heavy rain were observed during the period for sample D, cloud droplet scavenging with heavy rain might engender the reduction in soot particles that are internally mixed with soluble materials after hygroscopic growth into particles having larger diameters. Unfortunately, dried residual particles of fog droplets were not obtained in this study. A future direction of this study must be to study the respective mixing states of both interstitial and residual particles of fog droplets.

On the other hand, some water-insoluble ball-like particles (Fig. 4-4d) were observed in sample D, which comprised 7% of water-insoluble particles after dialysis (Type *a*). The relation between the particle diameter and the shadow length corresponded with that of a sphere particle. The spherical particles were not volatile after irradiation with strong electron beams. Considering the features of spherical morphology and electron beam resistance, these particles are probably either fly ash [*Mamane and Dzubay*, 1988] or tar balls [*Pósfai et al.*, 2004]. According to *Mamane and Dzubay* [1988], the fly ash particles contain Si and Al. The major element of tar balls is carbon [*Pósfai et al.*, 2004]. Based on analyses using SEM-EDX, the major element of the spherical particles in

sample D was C with less abundant O and Si after subtracting the carbon-covered collodion film (background), suggesting that the spherical particles in sample D are tar balls.

4.4. Factors controlling the mixing states of interstitial particles

The mixing states of water-soluble and water-insoluble materials for cloud interstitial and LG particles differed for the three fog events—A, D, and G—examined in this study. Activation of a particle as cloud condensation nuclei depends on size and chemical composition of the particle and conditions of water vapor saturation according to the Köhler theory [*Köhler*, 1936; *Pruppacher and Klett*, 1997]. The observed size ranges were the same for the three events. Therefore, the chemical composition of aerosols and conditions of water vapor saturation are considered to be controlling factors accounting for the difference in the mixing states. Although the Köhler theory is an equilibrium theory, particles under actual cloud forming conditions might not be in equilibrium, especially if film-forming organics are present on the particles [e.g., *Gill et al.*, 1983; *Bigg*, 1986; *Feingold et al*., 2002]. As pointed out in section 4.3, results of EDX analyses of samples A and G suggest that partly soluble particles contained not only sulfate but also organics, implying delay or suppression of cloud droplet formation for these samples. Unfortunately, details remain unknown for the organics found in samples A and D: it is unknown whether or not film forms on aerosol particles.

The mixing state of insoluble core and soluble material is another source of difference in interstitial particles. Figure 4-5 presents critical supersaturation for particles composed of an insoluble core and ammonium sulfate based on the Köhler theory. The critical supersaturations for 0.3 μm and 0.5 μm in dry diameter were

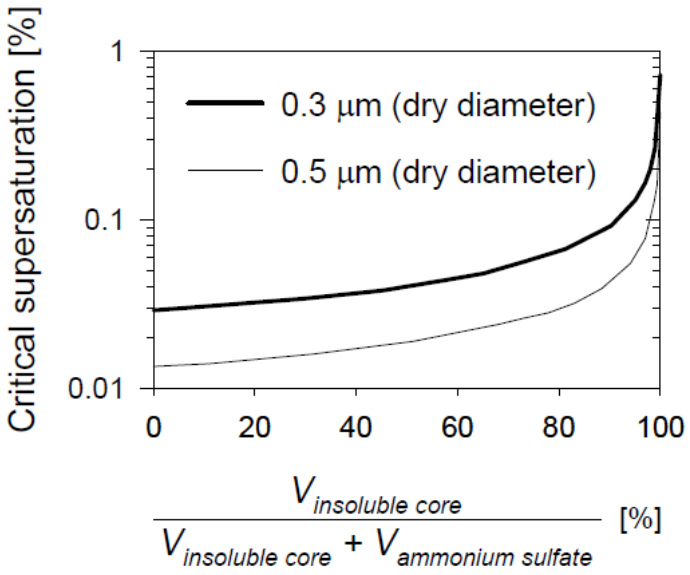

Figure 4-5 Relation between volume fraction of water-insoluble material and critical supersaturations. The critical supersaturations of water vapor are calculated for a particle of insoluble core with ammonium sulfate according to the Köhler theory. Thick and thin lines respectively show particles for 0.3 μm and 0.5 μm dry diameter.

calculated for various volume fractions of insoluble materials in internally mixed particles. Critical supersaturation for particles with a 100% insoluble core is estimated as 0.72% for 0.3 μm dry diameter. A particle with the same diameter but having an insoluble core fraction of 90% can be activated at much lower supersaturation of 0.09%. According to *Seinfeld and Pandis* [2006], realistic values of water-vapor supersaturation in the atmosphere are usually less than 1%; the median value is about 0.1%. As portrayed in Fig. 4-5, particles that can be activated at the critical supersaturation of 0.1% show insoluble fractions that are quite close to 100% for both sizes. Consequently, the dominance of interstitial particles without soluble material suggests the occurrence of meteorological conditions of higher (>0.1%) supersaturations.

To infer the relations between the mixing states of interstitial particles and water-vapor supersaturation, we will examine air trajectories and meteorological conditions related to cloud formation of air parcels that reached the observation site. Figure 4-6 portrays 24 hr horizontal and vertical backward trajectories of air parcels for samples A, D, and G starting from 2300 m and 3000 m above sea level at Mt. Tateyama, and hourly precipitation amounts along the trajectories. The backward trajectories and precipitation data were computed using the Hybrid Single-Particle Lagrangian Integrated Trajectory (HYSPLIT 4) model developed by the National Oceanic and Atmospheric Administration (NOAA) Air Resources Laboratory (ARL) [*Draxler and Rolph*, 2003; *Rolph*, 2003]. The beginning of the trajectory was set at every hour during the sample collection period. Horizontal air trajectories showed that the air masses of the fog events were derived mostly from the Pacific Ocean, moving clockwise to Mt. Tateyama, with the exception of sample G for 3000 m. The continental air mass might be partly mixed with oceanic air in the air mass from which sample G was collected. The vertical profiles of backward trajectories of the fog events indicated that the air

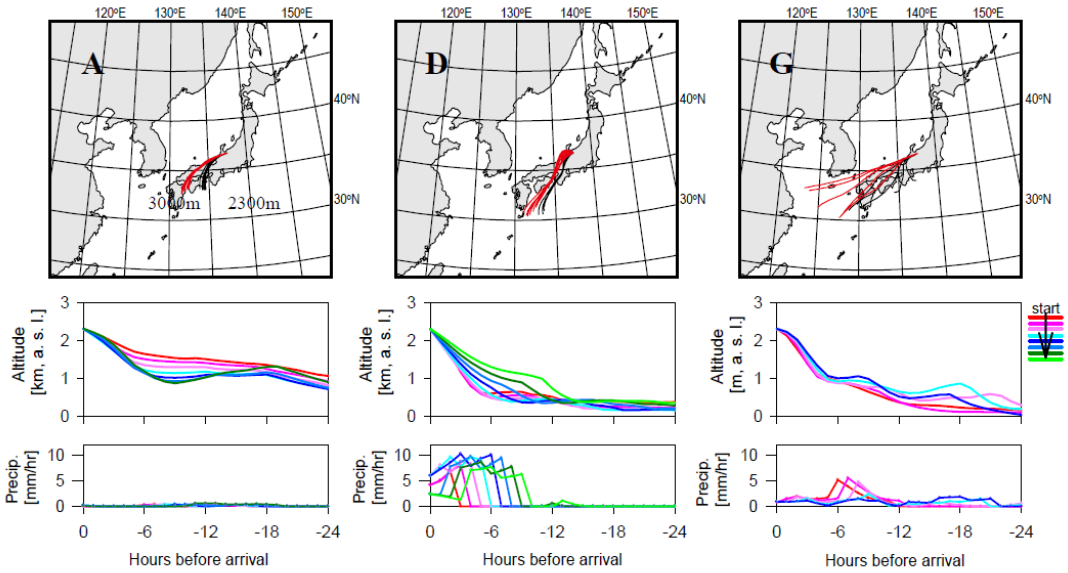

Figure 4-6 24-hr backward trajectory of air parcels and precipitation along the trajectories for samples A, D, and G. Upper row shows horizontal trajectory starting every hour during sample collection from altitudes at 2300 m a.s.l. (black lines) and 3000 m a.s.l. (red lines) over the observation site. Middle and lower rows respectively show vertical profiles of trajectories and hourly precipitation rates along trajectories starting every hour (red to green lines) from 2300 m a.s.l.

masses ascended from lower altitudes during the prior 24 hr with a steep gradient for the last 6 hr before arrival. Adiabatic cooling occurs in ascending air masses. Therefore, ascending motions of the air masses imply cloud formation. Estimated hourly precipitation for the last 6 hr before arrival were higher for sample D (> 7 mm/hr) than those of samples A and G, as shown in the lower panel of Fig. 4-6. Stronger precipitation during ascent implies the possibility of higher supersaturation experienced in clouds. In addition, as presented in Fig. 4-2a, local precipitation intensities observed at Kamiichi were quite different: high (2−6 mm/hr) for sample D but very low (ca. 1 mm/hr) for sample G. These results agree with the observed abundance of mostly insoluble particles (Type *a*) found in sample D and partially soluble particles (Type *c*) in samples A and G. Particles having water-soluble materials might not remain as interstitial particles in cloud for sample D because of higher supersaturation than that for samples A and G.

A similar tendency was reported for partitioning between cloud droplets and cloud interstitial particles at other high-elevation sites: soot particles remained in interstitial particles and sulfate particles were more likely to be scavenged to cloud droplets [*Hallberg et al.* 1992, 1994; *Kasper-Giebl et al.*, 2000; *Hitzenberger et al.*, 2001]. *Kasper-Giebl et al.* [2000], *Hitzenberger et al.* [2001], and *Cozic et al*. [2007] measured liquid water contents with soot concentration in clouds at mountain sites. They reported that fractions of interstitial soot of total (interstitial plus cloud droplets) soot concentrations decreased concomitantly with increasing liquid water content, but a fraction (20–40%) of interstitial soot remained under high liquid-water contents. The higher liquid-water contents that were found in their study might correlate with the higher precipitation amounts. Consequently, the existence of remaining interstitial soot particles is consistent with the presence of soot in sample D. As a new finding in our study, soot particles in cloud interstitial air under high precipitation conditions were

found only as externally mixed soot.

In this study, interstitial particles (0.1–0.5 μm) in fog with low precipitation intensity (samples A and G) were dominated by particles having water-soluble materials. The existence of soluble components in cloud interstitial particle was also observed in marine stratocumulus clouds with drizzle near San Diego (300 km offshore) [*Hawkins et al.*, 2008]. Because updraft velocities of clouds in their observation were not so high (mostly <1 m/s), the supersaturation in the clouds was also low, leading to inefficient activation of aerosol particles that were mixed internally with soluble materials. For non-precipitating clouds, *Twohy and Anderson* [2008] summarized results for phase partitioning of cloud droplet nuclei and aerosol particles using SEM and TEM. For smaller particles (<0.2 μm), salts (chlorides and sulfates) were preferentially incorporated to cloud droplets. Insoluble particles such as soot were activated only if they were mixed with sufficient soluble materials. In our study, with various precipitation intensities, internally mixed particles of soluble and insoluble materials were found as interstitial particles in low precipitation clouds, but interstitial particles under high precipitation conditions were mostly insoluble soot. For components such as soot in submicron particles, cloud-forming conditions (supersaturation) are more important as a factor controlling activation, in addition to the mixing states with soluble materials.

4. 5. Chapter summary

To investigate the mixing states of cloud interstitial particles, we observed aerosol particles through a fog cut inlet (<10 μm diameter) at Tengudaira (2300 m a.s.l.), Mt. Tateyama in Japan. The number concentration of LG particles (0.3−0.5 μm diameter)

was measured together with total particles (0.1−0.5 μm diameter). As an index of the abundance of LG particles, the number fraction of LG particles of 0.3−0.5 μm (F_{LG}) was calculated and used for aerosol sampling at the site. The LG particles were collected for analyses using water dialysis under TEM.

During fog conditions, the aerosol (>0.3 μm diameter) number concentration decreased about 1–2 orders of magnitude. Three samples of LG particles were collected under fog conditions as cloud interstitial samples for TEM analysis. In a sample under high F_{LG} values, most particles were found to be insoluble after water dialysis, suggesting that the value of F_{LG} depends on the number fraction of water-insoluble particles among all particles. This observation demonstrates the usefulness of real time F_{LG} monitoring to support aerosol sampling for time consuming individual particle analysis by TEM, and in turn, the representativeness of our samples. More than half of the insoluble particles were determined to be soot composed of chain aggregations of electron-opaque spherules. For the other two samples collected under fog conditions, low F_{LG} values were observed. Most particles of the two samples were partly water-soluble after water dialysis. Some particles were soot-containing particles mixed with organics and water-soluble materials.

To investigate the factors producing differences in the mixing states of interstitial particles, local precipitation intensity and meteorological situations en route were compared with the mixing states of particles. For the sample taken during higher local precipitation (2−6 mm/hr), most interstitial particles were water-insoluble soot particles with a few tar balls. In contrast, partly water-soluble particles were dominant in interstitial samples during low precipitation periods (ca. 1 mm/hr). In-cloud scavenging can change the population of soot-containing particles left behind in the atmosphere after precipitating a cloud, preferentially leaving soot particles without soluble materials

according to rain-forming conditions.

5. Changing processes of morphology and mixing states of soot-containing particles in the atmosphere

Previous sections presented morphology and mixing states of atmospheric soot-containing particles under different situations. The results of observation are helpful to improve our knowledge of changing processes of soot particles in the life cycle. Figure 5-1 shows a general life cycle of soot particles. Soot particles are largely emitted from fuel combustion and biomass burning. Soot particles by fossil fuels burning are emitted as mostly hydrophobic particles [*Weingartner et al.*, 1997; *Zuberi et al.*, 2005] and have chain-like shape as shown in Fig. 1-3. Such chain-like soot particles are often found at urban and sub-urban regions [e.g. *Hasegawa and Ohta*, 2002; *Adachi and Buseck*, 2008]. During transport in the atmosphere, aging processes can modify soot particles into particles internally mixed with the other materials (sulfate and organics, etc.), eventually enhancing the ability of acting as cloud condensation nuclei of the particle. If the soot-containing particle can be activated as cloud condensation nuclei with cloud formation, the soot-containing particles are scavenged into cloud droplets. After particles growing into cloud droplets, rain droplets efficiently removes the cloud droplets from the atmosphere to the earth's surface [*Pruppacher and Klett*, 1997]. Among these processes, this study has discussed about aging and scavenging processes. The observation results suggested the following changing processes of soot-containing particles in the atmosphere.

Figure 5-2 shows a schematic diagram of modifications of morphology and mixing states of soot-containing particles by aging processes. The features of observed soot-containing particles at Cape Hedo are depicted in dotted orange box in Fig. 5-2, as an aging consequence after transport from major source region. Most of soot-containing particles were internally mixed with large volume water-soluble materials.

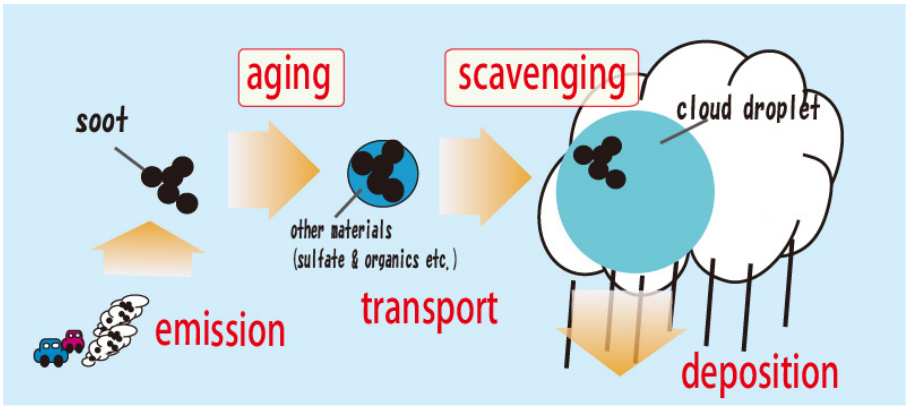

Figure 5-1 Life cycle of soot particles

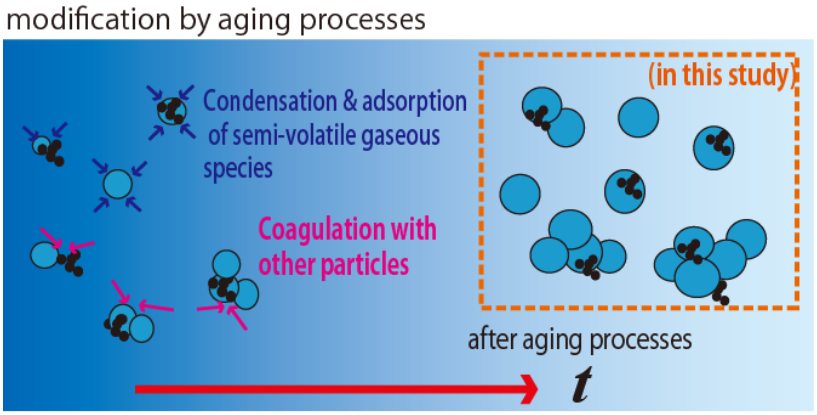

Figure 5-2 Schematic diagrams of modifications of morphology and mixing states of soot-containing particles by aging processes. Background blue shade indicates concentration graduation of aerosol precursor gases (e.g. SO_2 and NH_4).

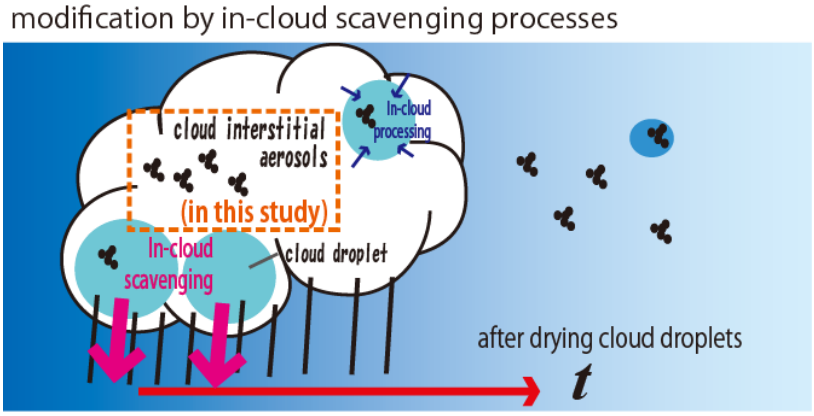

Figure 5-3 Schematic diagrams of modifications of mixing states of soot-containing particles by in-cloud scavenging processes. Background blue shade indicates concentration graduation of aerosol precursor gases (e.g. SO_2 and NH_4).

Soot-containing particles under dry conditions were mainly spheroid of 0.2–0.4 μm and larger clustered particles connecting multiple spheroids (about 0.3 μm in diameter). As already suggested by previous study, condensation and adsorption can modify soot particles into spheroidal particles internally mixed with soluble materials [*Zhang and Zhang*, 2005; *Pagels et al.*, 2009; *Khalizov et al.*, 2009a, 2009b]. This study further suggested that coagulation under high aerosol number concentration is also an effective process for evolutions of size, volume of soluble materials and morphology of the soot-containing particles. The increase of size and hygroscopicity also leads to enhancement of cloud-forming potential of the particle. Indeed, in cloud interstitial air at Mt. Tateyama, large soot-containing particles and hygroscopic particles were rare under high precipitation condition; most of cloud interstitial particles were soot particles without water-soluble materials having smaller sizes (<0.4 μm). Fig. 5-3 shows a schematic diagram of modifications of mixing states of soot-containing particles by in-cloud processes, which is led from an observed mixing state depicted in dotted orange box. After cloud drying, some of cloud droplet particles might be left with cloud processing, but precipitation efficiently remove cloud droplets from the atmosphere. On the other hand, cloud interstitial particles can be left in the atmosphere preferentially. In-cloud scavenging processes not only remove aerosol particles but also alter the external mixing states of particles left behind into the predominant states of hydrophobic soot. The surviving soot particles after scavenging processes might be transported for longer distances, with aging process under low aerosol concentrations.

Based on the morphology and mixing states of soot-containing particles, I have discussed about internal and external modifications of soot-containing particles. As explained in chapter 1, these modifications lead to variations of optical properties and spatial distribution of soot-containing particles in the atmosphere. In addition to

modification of condensation already known, the formation of coagulated particles under high aerosol concentration conditions and the change in mixing states after in-cloud scavenging should be considered as key processes in evaluation of climatic effect by soot-containing particles.

6. Summary and conclusions

Morphology and mixing states of soot-containing particles are important information for considering optical and physicochemical properties and climate effects of soot-containing particles in the atmosphere. To elucidate relations between morphological features of soot-containing particles and aging and in-cloud scavenging processes, aerosol and soot-containing particles were observed at two sites. Two observations were made at Cape Hedo, located at Okinawa as leeward area of East Asia, and in cloud situation at Tengudaira (2300 m a.s.l.), Mt. Tateyama. For particles and soot-containing particles in samples collected at each observation, morphological features and mixing states with water-soluble materials were observed by using an electron microscope analysis with water dialysis method.

Atmospheric aerosol particles in continental outflow from East Asia were observed at Cape Hedo. Six samples of aerosol particles derived from eastern central China in 1-5 days were analyzed for morphological features and mixing states of soot-containing particles (0.2–0.7 μm) by water dialysis under TEM observation. Number proportions of the soot-containing particles ranged from 2% to 25% for 0.2–0.4 μm and 14% to 59% for 0.4–0.7 μm. Most of soot-containing particles were internally mixed with large volume (>80%) of soluble materials. The insoluble core diameters in soot-containing particles of 0.2–0.4 μm and 0.4–0.7 μm were almost same (0.1–0. 25 μm). Results of EDX elemental analysis on individual particles and Q-AMS aerosol chemical measurements at the site suggested that soluble materials in samples mainly consisted of SO_4^{2-}, organics and NH_4^+. For samples consisted mainly of ammonium sulfate and organics, soot-containing particles were ball-like shape or cocoon-like shape for 0.2–0.4 μm, and clustered shape connecting multiple units (about 0.3 μm in diameter) for larger size range. The shape and size of a single unit of cluster-like particle were similar to those of ball-like particles or

cocoon-like particles in the same sample, implying formation of cluster-like particles by coagulation process. The number proportions of coagulated particles to total particles were estimated with appropriate initial conditions adapting to our observation. Number concentration of coagulated particles estimated using a simple coagulation model reasonably agreed with observed number proportion of cluster-like particles. This suggests that coagulation cluster might also important for aerosol size evolution in polluted atmosphere.

To investigate modification of soot-containing particle population after wet scavenging process, cloud interstitial particles through a fog cut inlet (<10 μm diameter) were observed at Tengudaira (2300 m a.s.l.), Mt. Tateyama. During fog conditions, the aerosol (>0.3 μm diameter) number concentration decreased about 1–2 orders of magnitude. During fog condition with higher local precipitation (2−6 mm/hr), F_{LG} values and soot-volume fraction in total aerosol were high. Most of particles in samples of cloud interstitial LG particles were found to be insoluble after water dialysis. More than half of the insoluble particles were determined to be soot composed of chain aggregations of electron-opaque spherules. On the other hand, under fog conditions with low precipitation periods (ca. 1 mm/hr), low F_{LG} values were observed. Most of particles in the samples of cloud interstitial LG particles were partly water-soluble after water dialysis. Some particles were soot-containing particles mixed with organics and soluble materials. In-cloud scavenging can change the population of particles left behind in the atmosphere, preferentially leaving water-insoluble particles according to cloud-forming conditions.

Based on the observation results of morphology and mixing states of soot-containing particles, this study discussed about changing processes of soot-containing particles in the life cycle. In addition to condensation process known already, modification with

coagulation process under high aerosol concentration and change of mixing states with in-cloud scavenging process are suggested as key processes controlling size, volume of soluble materials and morphological features of soot-containing particles in the atmosphere.

Acknowledgments

I am grateful to Dr. K. Osada for valuable guidance and continuous encouragements. I would like to thank Prof. T. Shibata for discussions and useful suggestions. Many thanks to the present and former members of our laboratory Drs. C. Nishita-Hara and J. Li, and Misses. N. Kawakami, Y. Shido, S. Ura and M. Kagawa and Messrs. Y. Komatsubara, K. Kawakita, and Y. Mizuno. I wish to express gratitude to Dr. K. Okada of the Meteorological Research Institute for guidance and advice throughout this study, especially with respect to the water dialysis method. I am indebted to staff members of the Tengudaira Sanso, and Mr. H. Iida and staff members of Tateyama Caldera SABO Museum for assisting our work at Mt. Tateyama. I am indebted to Prof. A. Takami and Mr. Y. Takeda of CHAAMS at Cape Hedo aerosol observation station. I wish to express gratitude to Mr. T. Goto at the Technical Center of Nagoya University for technical advices on electron microscopy and Prof. Koyama at Nagoya University for lending the electron microscopy. I wish to thank Dr. Shiobara at National Institute of Polar Research for lending PSAP.

Data on sulfur dioxide at Cape Hedo were provided by MOE ADORC. I gratefully acknowledge the NOAA Air Resources Laboratory (ARL) for providing the HYSPLIT transport model (http://www.arl.noaa.gov/ready.html).

References

Adachi, K., S. H. Chung, and P. R Buseck (2010), Shapes of soot aerosol particles and implications for their effects on climate, *J. Geophys. Res.*, *115*, D15206, doi:10.1029/2009JD012868.

Andreae, M. O., and D. Rosenfeld (2008), Aerosol-cloud-precipitation interactions: Part 1. The nature and sources of cloud-active aerosols, *Earth Sci. Rev.*, *89*, 13– 41.

Acker, K., Mertes, S., Möller, D., Wieprecht, W., Auel, R., Kalaß, D., 2002. Case study of cloud physical and chemical processes in low clouds at Mt. Brocken, Atmos. Res., 64, 41–51.

Bigg, E. K., 1986. Discrepancy between observations and prediction of concentrations of cloud condensation nuclei, Atmos. Res., 20, 82–86.

Bond, T. C., D. G. Streets, K. F. Yarber, S. M. Nelson, J.-H. Woo and Z. Klimont (2004), A technology-based global inventory of black and organic carbon emissions from combustion, *109*, D14203, dou: 10.1029/2003JD003697.

Bond, T. C. and R. W. Bergstrom (2006), Light absorption by carbonaceous particles: an investigative review, *Aerosol Sci. Technol.*, *40*, 27–67.

Bond, T. C. E. Bhardwaj, R. Dong, R. Jogani, S. Jung, C. Roden, D. G. Streets, and N. M. Trautmann (2007), Historical emissions of black and organic carbon aerosol from energy-related combustion, 1850–2000. *Global Biogeochem. Cycles* 21, doi:10.1029/2006GB002840.

Buseck, P. R., and M. Pósfai (1999), Airborne minerals and related aerosol particles: Effects on climate and environment, *Proc. Natl. Acad. Sci. USA, 96,* 3372–3379.

Chung, C. E., V. Ramanathan, D. Kim and I. A. Podgorny (2005), Global anthropogenic aerosol direct forcing derived from satellite and ground-based observations, *J. Geophys.Res.*, *110*, D24207, doi:10.1029/2005JD006356.

Cozic, J., B.Verheggen., S.Mertes, P. Connolly, K. Bower, A. Petzold, U. Baltensperger, and E. Weingartner (2007), Scavenging of black carbon in mixed phase clouds at the high alpine site Jungfraujoch, *Atmos. Chem. Phys., 7*, 1797–1807.

Croft, B., U. Lohmann, and K. von Salzen (2005), Black carbon aging in the Canadian centre for climate modeling and analysis atmospheric general circulation

model, *Atmos. Chem. Phys., 5*, 1931–1949.

Draxler, R. R., and G. D. Rolph (2003), HYSPLIT (HYbrid Single-Particle Lagrangian Integrated Trajectory) Model access via NOAA ARL READY Website (http://www.arl.noaa.gov/ready/hysplit4.html), NOAA Air Resources Laboratory, Silver Spring, MD.

Feingold, G. and P. Y. Chuang (2002), Analaysis of influence of film-forming compounds on droplet growth: implications for cloud microphysical processes and climate, *J. Atmos. Sci.*, 59, 2006–2018.

Ferek, R. J., A. L. Lazrus, and J. W. Winchester (1983), Electron microscopy of acidic aerosols collected over the northeastern United State, *Atmos. Environ.*, *17*, 1545–1561.

Fuchs, N. A (1964), The coagulation of aerosols, in *The mechanics of aerosols*, pp. 288–322, Dover Publications, Inc., New York.

Fuller, K. A., W. C. Malm and Kreidenweis, S. M. (1999), Efects of mixing on extinction by carbonaceous particles, *J. Geophys. Res.*, *104*(D13), 15941–15954.

Gelencsér, A. (2004), *Carbonaceous aerosol, Atmospheric and Oceanographic Sciences Library,* vol. 30, 350 pp., Springer, Netherlands.

Gill, P. S., Graedel, T. E. and C. J. Weschler (1983), Organic films on atmospheric aerosol particles, fog droplets, cloud droplets, raindrops, and snowflakes, *Rev. Geopys.*, 21, 903–920.

Gras, J. L. and G. P. Ayers (1979), On sizing impacted sulfuric acid aerosol particles, *J. Appl. Meteor.*, *18*, 634–638.

Hallberg, A., J. A. Ogren, K. J. Noone, J. Heintzenberg, A. Berner, I. Solly, C. Kruisz, G. Reischl, S. Fuzzi, M. C. Facchini, H.-C. Hansson, A. Wiedensohler, and I. B. Svenningsson (1992), Phase partitioning for different aerosol species in fog, *Tellus, 44B*, 545–555.

Hallberg, A., J. A. Ogren, K. J. Noone, K. Okada, J. Heintzenberg, and I. B. Svenningsson (1994), The influence of aerosol particle composition on cloud droplet formation, *J. Atmos. Chem., 19*, 153–171.

Hand, J. L. W. C. Malm, A. Laskin, D. Day,1 T. Lee, C. Wang, C. Carrico, J. Carrillo, J.

P. Cowin, J. Collett Jr. and M. J. Iedema (2005), Optical, physical, and chemical properties of tar balls observed during the Yosemite Aerosol Characterization Study, *J. Geophys. Res*., *110*, D21210, doi:10.1029/2004JD005728.

Hansen, A. D. A., H. Rosen, and T. Novakov (1984), The aethalometer – An instrument for the real time measurement of optical absorption by aerosol particles, *Sci. Total Environ., 36*, 103-110.

Hansen, J., and L. Nazarenko (2004), Soot climate forcing via snow and ice albedos, *Proc. Natl. Acad. Sci., 101,* 423–428.

Hasegawa. S., and S. Ohta (2002), Some measurements of the mixing state of soot-containing particle at urban and non-urban sites, *Atmos. Environ., 36*, 3899–3908.

Hawkins, L. N., L. M. Russell, C. H. Twohy, and J. R. Anderson (2008), Uniform particle-droplet partitioning of 18 organic and elemental components measured in and below DYCOMS-II stratocumulus clouds, *J. Geophys. Res., 113*, D14201, doi:10.1029/2007JD009150.

Haywood, J.M., D.L. Roberts, A. Slingo, J.M. Edwards and K.P. Shine (1997), General circulation model calculations of the direct radiative forcing by anthoropogenic sulfate and fossil-fuel soot aerosolm, *J. Climate*, *10*, 1562–1577.

Haywood, J. M., and O. Boucher (2000), Estimate of the direct and indirect radiative forcing due to tropospheric aerosols: A review, *Reviews of Geophys., 38,* 513–543.

Hinds, C. H. (1999), Straight-line acceleration and curvilinear particle motion, in *Aerosol Technology,* 2nd ed., pp. 111–140, John Wiley and Sons, Inc., New York.

Hitzenberger, R., A. Berner, R. Kromp, A. Kasper-Giebl, A. Limbeck, W. Tscherwenka, and H. Puxbaum (2000), Black carbon and other species at a high-elevation European site (Mount Sonnblick, 3106 m, Austria), Concentrations and scavenging efficiencies, *J. Geophys. Res., 105*(D20), 24637–24645.

Hitzenberger, R. and S. Tohno (2001), Comparison of black carbon (BC) aerosols in two urban areas – concentrations and size distributions, *Atmos. Enviton.*, *35*,

2153–2167.

Hitzenberger, R., A. Berner, H. Giebl, K. Drobesch, A. Kasper-Giebl, M. Loeflund, H. Urban, and H. Puxbaum (2001), Black carbon (BC) in alpine aerosols and cloud water – concentrations and scavenging efficiencies, *Atmos. Environ., 35*, 5135–5141.

Huang, X. F., J. Z. Yu, L. Y. He, and M. Hu (2006), Size distribution characteristics of elemental carbon emitted from Chinese vehicles: Results of a tunnel study and atmospheric implications, *Environ. Sci. Technol., 44*, 5355–5360.

Huang, X. F., and J. Z. Yu (2008), Size distribution characteristics of elemental carbon in the atmosphere of coastal urban area in South China: characteristics, evolution processes, and implications for the mixing state, *Atmos. Chem. Phys., 8*, 5843–5853.

Husar, R. B. and K. T. Whitby (1973), Growth Mechanisms and size spectra of photochemical aerosols, *Environ. Sci. Technol.*, *7*, 241–247.

Intergovernmental Panel on Climate Change (IPCC) (2007), *Climate Change 2007: The Scientific Basis. Contribution of Working Group I to the Fourth Assessment Report of the Intergovernmental Panel on Climate Change*, edited by S. Solomon et al., Cambridge Univ. Press, New York.

Jacobson, M. Z (2001), Strong radiative heating due to the mixing state of black carbon in atmospheric aerosols, *Nature*, *409*, 695–697.

Janzen, J. (1980), Extinction of light by highly nonspherical strongly absorbing colloidal particles: spectrophotometric determination of volume distributions for carbon blacks, *Appl. Opt., 19*, 2977–2985.

Junge, C. E. (1963), *Air Chemistry and Radioactivity*, pp. 382., Academic Press, New York.

Kasper-Giebl, A., A. Koch, R. Hitzenberger, and H. Puxbaum (2000), Scavenging efficiency of ‘aerosol carbon’ and sulfate in supercooled clouds at Mt. Sonnblick (3106 m a.s.l., Austria), *J. Atmos. Chem., 35*, 33–46.

Kaneyasu, N. and S. Murayama (2000), High concentrations of black carbon over middle latitudes in the North Pacific Ocean, *J. Geophys. Res.*, *105*(D15), 19881–19890.

Kleinman, L. I., S. R. Springston, J. Wang, P. H. Daum, Y.-N. Lee, L. J. Nunermacker, G. I. Senum, J. Weinstein-Lloyd, M. L. Alexander, J. Hubbe, J. Ortega, R. A. Zaveri, M. R. Canagaratna and J. Jayne (2009), The time evolution of aerosol size distribution over the Mexico City plateau, *Atmos. Chem. Phys.*, *9*, 4261–4278.

Khalizov, A. F., H. Xue , L. Wang, J. Zheng and R. Zhang (2009a), Enhanced light absorption and scattering by carbon soot aerosol internally mixed with sulfuric acid, *J. Phys. Chem.*, *113*, 1066–1074.

Khalizov, A. F., R. Zhang, D. Zhang, H. Xue, J. Pagels and P. H. McMurry (2009b), Formation of highly hygroscopic soot aerosols upon internal mixing with sulfuric acid vapor, *J. Geophys. Res*., *114*, D05208, doi:10.1029/2008JD010595.

Koch, D. (2001), Transport and direct radiative forcing of carbonaceous and sulfate aerosols in the GISS GCM, *J. Geophys. Res., 106*(D17), 20311–20332.

Koch, D., and J. Hansen (2005), Distant origins of Arctic black carbon: A Goddard Institute for Space Studies Model E experiment, *J. Geophys. Res., 110,* D04204, doi:10.1029/2004JD005296.

Köhler, H. (1936), The nucleus in and the growth of hygroscopic droplets, *Trans. Faraday Soc., 32*, 1152–1161.

Lack, D. A. and C. D. Cappa (2010), Impact of blown and clear carbon on light absorption enhancement, single scatter albedo and absorption wavelength dependence of black carbon, *Atmos. Chem. Phys*., *10*, 4207–4220.

Li, J., M. Posphai, P. V. Hobbs and P. R. Buseck (2003), Individual aerosol particles from biomass burning in southern Africa: 2, Compositions and aging of inorganic particles, *J. Geophys. Res*., *108*(D13), 8484, doi:10.1029/2002JD002310.

Li, W. and L. Shao (2010), Mixing and water-soluble characteristics of particulate organic compounds in individual urban aerosol particles, *J. Geophys. Res*., *115*, D02301, doi:10.1029/2009JD012575.

Liu, B. Y. H., D. Y. H. Pui, K. T. Whitby and D. B. Kittelson (1978), The aerosol mobility chromatograph: a new detector for sulfuric acid aerosols, *Atmos. Environ.*, *12*, 99–104.

Mamne, Y., and T. G. Dzubay (1988), Fly ash concentration in Philadelphia aerosol determined by electoron microscopy, *Water, Air and Soil Pollut., 37,* 389–405.

Mamane, Y. and J. Gottlieb (1989), The study of heterogeneous reactions of carbonaceous particles with sulfur and nitrogen oxides using a single particles, *J. Aerosol. Sci.*, *20*, 575–584.

Meng, Z. and J. H. Seinfeld (1994), On the source of submicrometer droplet mode of urban and regional aerosols, *Aerosol Sci. Technol*, *20*, 253–265.

Meng, Z.-Y., X.-B. Xu, T. Wang, X.-Y. Zhang, X.-L. Yu, S.-F. Wang, W.-L. Lin, Y.-Z. Chen, Y.-A. Jiang and A.-Q. An (2010), Ambient sulfur dioxide, nitrogen dioxide, and ammonia at ten background and rural sites in China during 2007–2008, *Atmos. Environ.*, *44*, 2625–2631.

Mossop, S. C. (1963), Stratspheric particles at 20 km, *Nature, 199*, 325–326.

Moteki, N., Y. Kondo, Y. Miyazaki, N. Takegawa, Y. Komazaki, G. Kurata, T. Shirai, D. R. Blake, T. Miyakawa and M. Koike (2007), Evolution of mixing state of black carbon particles: aircraft measurements over the western Pacific in March 2004, *Geophys. Res. Lett. 34*, L11803, doi:10.1029/2006GL028943.

Murr, L. E., and K. F. Soto (2005), A TEM study of soot, carbon nanotubes, and related fullerene nanopholyhedra in common fuel-gas combustion sources, *Mater. Charact., 55,* 50–65.

Naoe, H., and K. Okada (2001), Mixing properties of submicrometer aerosol particles in the urban atmosphere –with regard to soot particles, *Atmos. Environ., 35*, 5765–5772.

Nakajima, T., S.-C. Yoon, V. Ramanathan, G.-Y. Shi,T. Takemura, A. Higurashi, T. Takamura, K. Aoki, B.-J. Sohn, S.-W. Kim, H. Tsuruta, N. Sugimoto, A. Shimizu, H. Tanimoto, Y. Sawa, N.-H. Lin, C.-T. Lee, D. Goto and N. Schutgens (2007), Overview of the Atmospheric Brown Cloud East Asian Regional Experiment 2005 and a study of the aerosol direct radiative forcing in east Asia, *J. Geophys. Res.*, *112*, D24S91, doi:10.1029/2007JD009009.

Novakov, T., V. Ramanathan, J. E. Hansen, T. W. Kirchstetter, M. Sato, J. E. Sinton, and J. A. Sathaye (2003), Large historical changes of fossil-fuel black carbon aerosols. *Geophys. Res. Lett,* 30, doi:10.1029/2002GL016345.

Ogren, J. A., and R. J. Charlson (1983), Elemental carbon in atmosphere: cycle and lifetime, *Tellus, 35B*, 241–254.

Ohara, T., H. Akimoto, J. Kurokawa, N. Horii, K. Yamaji, X. Yan and T. Hayasaka (2007), An Asian emission inventory of anthropogenic emission sources for the period 1980–2020, *Atmos. Chem. Phys.*, *7*, 4419–4444.

Okada. K. (1983), Nature of individual hygroscopic particles in the urban atmosphere, *J. Meteor. Soc. Japan., 61*, 727–735.

Okada, K., and R. M. Hitzenberger (2001), Mixing properties of individual submicrometer aerosol particles in Vienna, *Atmos. Environ., 35*, 5617–5628.

Okada, K., M. Ikegami, Y. Zaizen., Y. Makino., J. B. Jensen, and J. L. Gras (2001), The mixture state of individual aerosol particles in the 1997 Indonesian haze episode, *J. Aerosol. Sci., 32*, 1269–1279.

Osada, K., M. Kido, H. Iida, K. Matsunaga, Y. Iwasaka, M. Nagatani, and H. Nakada (2003), Seasonal variation of free tropospheric aerosol particles at Mt. Tateyama, central Japan. *J. Geophys. Res., 108*(D23), doi:10.1029/2003JD003544.

Osada, K., M. Kido, C. Nishita, K. Matsunaga, Y. Iwasaka, M. Nagatani, and H. Nakada (2007), Temporal variation of water soluble ions of free tropospheric aerosol particles over central Japan, *Tellus, 59B*, 742–754.

Pagels, J., A. F. Khalizov, P. H. McMurry and R. Y. Zhang (2009), Processing of soot by controlled sulphuric acid and water condensation—Mass and mobility relationship, *Aerosol Sci. Technol*, *43*, 629–640.

Pilinis, C., S. N. Pandis, and J. H. Seinfeld (1995), Sensitivity of direct climate forcing by atmospheric aerosols to aerosol size and composition, *J. Geophys. Res., 100*(D9), 18739–18754.

Pósfai, M., J. R. Anderson, P. R. Buseck and H. Sievering (1999), Soot and sulfate aerosol particles in the remote marine troposphere, *J. Geophys. Res.*, *104*(D17), 21685–21693.

Pósfai, M., A. Gelencser, R. Simonics, K. Arato, J. Li, P. V. Hobbs, and P. R. Buseck (2004), Atmospheric tar balls: Particles from biomass and biofuel burning, *J. Geophys. Res., 109,* D06213, doi: 10.1029/2003JD004169.

Pruppacher, H. R., and J. D. Klett (1997), *Microphysics of clouds and precipitation, Second revised and enlarged edition with introduction to cloud chemistry and cloud electricity*, 954 pp., Kluwere Academic Publishers, Dordrecht/ Boston/ London.

Ramanathan, V., F. Li, M. V. Ramana, P. S. Praveen, D. Kim, C. E. Corrigan, H. Nguyen, E. A. Stone, J. J. Schauer, G. R. Carmichael, B. Adhikary, and S. C. Yoon (2007), Atmospheric brown clouds: Hemispherical and regional variations in long-range transport, absorption, and radiative forcing, *J. Geophys. Res.*, *112*, D22S21, doi:10.1029/2006JD008124.

Ramanathan, V., and G. Carmichael (2008), Global and regional climate changes due to black carbon, *Nature Geoscience, 1*, 221–227.

Rolph, G. D. (2003), Real-time environment applications and display system (READY), NOAA Air Resour. Lab., Silver Spring, Md. (Available at http://www.arl.noaa.gov/ready/hysplit4.html)

Schwarz, J. P., J. R. Sparkman, D. W. Fahey, R. S. Gao, U. Lohmann, P. Stier, L. A. Watts, D. S. Thomson, D. A. Lack, L. Pfister, M. J. Mahoney, D. Baumgardner, J. C. Wilson and J. M. Reeves (2008), Coating and their enhancement of black carbon light absorption in the tropical atmosphere, *J. Geophys. Res*., *113*, D03203, doi:10.1029/2007JD009042.

Seinfeld, J. H., and S. N. Pandis (2006), *Atmospheric Chemistry and Physics, From Air Pollution to Climate Change,* 2nd ed., 1203 pp., John Wiley and Sons, Inc., New York.

Slinn, W. G. N. (1983), Precipitation scavenging, in *Atmospheric Sciences and Power Production–1979*, Chap. 11, Division of Biomedical Environmental Research, U. S. Depertment of Energy, Washington, DC.

Stier, P., J. H. Seinfeld, S. Kinne, J. Feichter, and O. Boucher (2006), Impact of nonabsorbing anthropogenic aerosols on clear-sky atmospheric absorption, *J. Geophy. Res., 111*, D18201, doi:10.1029/2006JD007147.

Streets, D.G., T. C. Bond, G. R. Carmichael, S. D. Fernandes, Q. Fu, D. He, Z. Klimont, S. M. Nelson, N. Y. Tsai, M. Q. Wang, J.-H. Woo and K. F. Yarber (2003), An inventory of gaseous and primary aerosol emissions in Asia in the year 2000, *J. Geophys. Res.*, *108*(D21), 8809, doi:10.1029/2002JD003093.

Swietlicki, E., J. Zhou, O. H. Berg, B. G. Martinsson, G. Frank, S.-I. Cederfelt, U. Dusek, A. Berner, W. Birmili, A. Wiedensohler, B. Yuskiewicz and K. N. Bower (1999), A closure study of sub-micrometer aerosol particle hygroscopic behaviour, *Atmos. Res.*, 50, 205–240.

Swietlicki, E., H.-C. Hansson, K. Hämeri, B. Svenningsson, A. Massling, G. Mcfiggans, P. H. McMurry, T. Petäjä, , P. Tunved, M. Gysel, D. Topping, E. Weingartner, U. Baltensperger, J. Rissler, A. Wiedensohler and M. Kulmala (2008), Hygroscopic properties of submicrometer atmospheric aerosol particles measured with H-TDMA instruments in various environments—a review, Tellus, 60B, 432–469.

Tang, I. N., and H. R. Munkelwitz (1993), Composition and temperature dependence of the deliquescence properties of hygroscopic aerosols, *Atmos. Environ., 27A*, 467–473.

Takami, A., T. Miyoshi, A. Shimono, N. Kaneyasu, S. Kato, Y. Kajii, and S. Hatakeyama (2007), Transport of anthropogenic aerosols from Asia and subsequent chemical transformation, *J. Geophys. Res*., *112*, D22S31, dio:10.1029/2006JD008120.

Takiguchi, Y., A. Takami, X. Lun, A. Shimizu, I. Matsui, N. Sugimoto, W. Wang, H. Bandow and S. Hatakeyama (2008), Transport and transformation of total reactive nitrogen over the East China Sea, *J. Grophys. Res.*, *113*, D10306, doi:10.1029/2007JD009462.

Twohy, C. H. and J. R. Anderson (2008), Droplet nuclei in non-precipitating clouds: composition and size matter, *Environ. Res. Lett., 3*, 1–9.

Twomey, S. (1977), *Atmospheric Aerosols*, *Developments in Atmospheric Science,* vol. 7, 302 pp., Elsevier, New York.

Venkataraman, C. and S. Friendlander (1994), Size distribution of polycycllc aromatic hydrocarbons and elemental carbon. 2. ambient measurements and effects of atmospheric processes, *Environ. Sci. Technol.*, *28*, 563–572.

Vester, B. P., M. Ebert, E. B. Barnert, J. Schneider, K. Kandler, L. Schütz and S. Weinbruch (2007), Composition and mixing state of the urban background aerosol in the Rhein-Main area (Germany), *Atmos. Environ.*, *41*, 6102–6115.

Weingartner. E., H. Burtscher, and U. Baltensperger (1997), Hygroscopic properties of

carbon and diesel soot particles, *Atmos. Environ.*, 31, 2311–2327.

Worringen A., M. Ebert, T. Trautmann, S. Weinbruch and G. Helas (2008), Optical properties of internally mixed ammonium sulfate and soot particles–a study of individual aerosol particles and ambient aerosol populations, *Appl. Opt.*, *47*, 3835–3845.

Wu, Z., M. Hu, P. Lin, S. Liu, B. Wehner and A. Wiedensohler (2008), Particle number size distribution in the urban atmosphere of Beijing, China, *Atmos. Environ*., *42*, 7967–7980.

Zuberi, B., K. S. Johnson, G. K. Aleks, L. T. Molina, and M. J. Molina (2005), Hydrophilic properties of aged soot, *Geophys. Res. Lett., 32(L01807)*, doi:10.1029/2004GL021496.

副　論　文

1. Mixing states of cloud interstitial particles between water-soluble and insoluble insoluble materials at Mt. Tateyama, Japan: effects of meteorological conditions,
Ueda, S., K. Osada and K. Okada,
Atmospheric Research, volume 99, Issue 2, pp325–336, February 2011

2. Morphological features of soot-containing particles internally mixed with water-soluble materials in continental outflow observed at Cape Hedo Okinawa, Japan
Ueda, S., K. Osada and A. Takami
（2010年12月にJournal of Geophysical Researchへ投稿）

参 考 論 文

1. 都心における大気エアロゾル粒子の湿度特性の季節変化
上田紗也子、三浦和彦
大気環境学会誌、第 42 巻、第 6 号、pp339–349、2007 年 11 月